UNIVERSITY OF CALIFORNIA
RIVERSIDE

Graphene-Enhanced Thermal Interface Materials for Thermal Management of Solar Cells

A Dissertation submitted in partial satisfaction
of the requirements for the degree of

Doctor of Philosophy

in

Electrical Engineering

by

Mohammed Ahmed Saadah

September 2017

Dissertation Committee:

Dr. Alexander A. Balandin, Chairperson
Dr. Roger Lake
Dr. Alexander Khitun

The Dissertation of Mohammed Ahmed Saadah is approved by:

Committee Chairperson

University of California, Riverside

Acknowledgments

First, I wish to express my sincere appreciation to my advisor, Dr. Alexander Balandin for giving me the honor of working under his supervision, and for lending valuable support in the course of my study and research, I will always be indebted to you and you will always be my greatest mentor. A very special thanks goes out to my Dissertation committee, Dr. Roger Lake and Dr. Alexander Khitun for their assistance and support. I would also to thank my colleagues and friends for a group of amazing people! Especially Ruben Salgado, Edward Hernandez, Chenglong Jiang, and Rameez Samnakay. It was great sharing the laboratory with all of you and I will remember our days together forever. A very special gratitude goes out to the King Abdullah Scholarship Program, the University of California – Riverside, and the Department of Electrical and Computer Engineering at Bourns College of Engineering. Last but not the least, I am grateful to my father; Ahmed Sadah who supported and encouraged me and for being the source of my inspiration, my mother; Khadija Alghamdi for her continuous unconditional love, my wife and children their love and patience, and all my brothers and sisters. Thank you all for your patience and spiritual support through my years of studies.

ABSTRACT OF THE DISSERTATION

Graphene-Enhanced Thermal Interface Materials for Thermal Management of Solar Cells

by

Mohammed Saadah

Doctor of Philosophy, Graduate Program in Electrical Engineering

University of California, Riverside, September 2017

Dr. Alexander Balandin, Chairperson

The interest to photovoltaic solar cells as a source of energy for a variety of applications has been rapidly increasing in recent years. Solar cells panels that employ optical concentrators can convert more than 30% of absorbed light into electricity. Most of the remaining 70% of absorbed energy is turned into heat inside the solar cell. The increase in the photovoltaic cell temperature negatively affects its power conversion efficiency and lifetime. In this dissertation research I investigated a feasibility of using graphene fillers in thermal interface materials for improving thermal management of multi-junction concentrator solar cells. Graphene and few-layer graphene fillers, produced by a scalable environmentally-friendly liquid-phase exfoliation technique, were incorporated into conventional thermal interface materials. Characteristics of the composites have been

examined with Raman spectroscopy, optical microscopy and thermal conductivity measurements. Graphene-enhanced thermal interface materials have been applied between a solar cell and heat sink to improve heat dissipation. The performance of the single and multi-junction solar cells has been tested using an industry-standard solar simulator under the light concentration of up to 2000 suns. It was found that the application of graphene-enhanced thermal interface materials allows one to reduce the solar cell temperature and increase the open-circuit voltage. We demonstrated that the use of graphene helps in recovering significant amount of the power loss due to solar cell overheating. The obtained results are important for the development of new technologies for thermal management of concentrated and multi-junction photovoltaic solar cells.

Table of Contents

List of Figures

List of Tables

Introduction

1.1 Motivations

The photovoltaic solar cell is an electronic device that generates electricity directly from the sunlight using a phenomenon called the photovoltaic effect. This phenomenon was first observed by French scientist Edmond Becquerel in 1839. The first silicon photovoltaic cell emerged in 1954 at Bell Labs in the United States [1]. This great advancement in technology has marked the beginning of the end for the use of conventional fossil fuel energy and the gradual shift to using clean renewable energy. While that PV cell had only 6% conversion efficiency, which means it only converts 6% of the incident solar light energy into electrical output, the advancement in the field has helped improved that efficiency much closer to the Shockley–Queisser theatrical limit of 33.7% efficiency for a single p-n junction silicon PV cell under 1 sun concentration, Figure 1.1 [2]. The amount of sun energy reaching earth in one hour is more than the world's annual consumption [3]. With the dawn of the 21st century, many countries have started building PV solar cities reaching a global capacity of 302 gigawatts in 2016. The PV growth in global capacity has been almost 30% every year for the last 3 years and is projected to reach 500 gigawatts by 2020 with oil dependent countries announcing their own solar power projects [4].

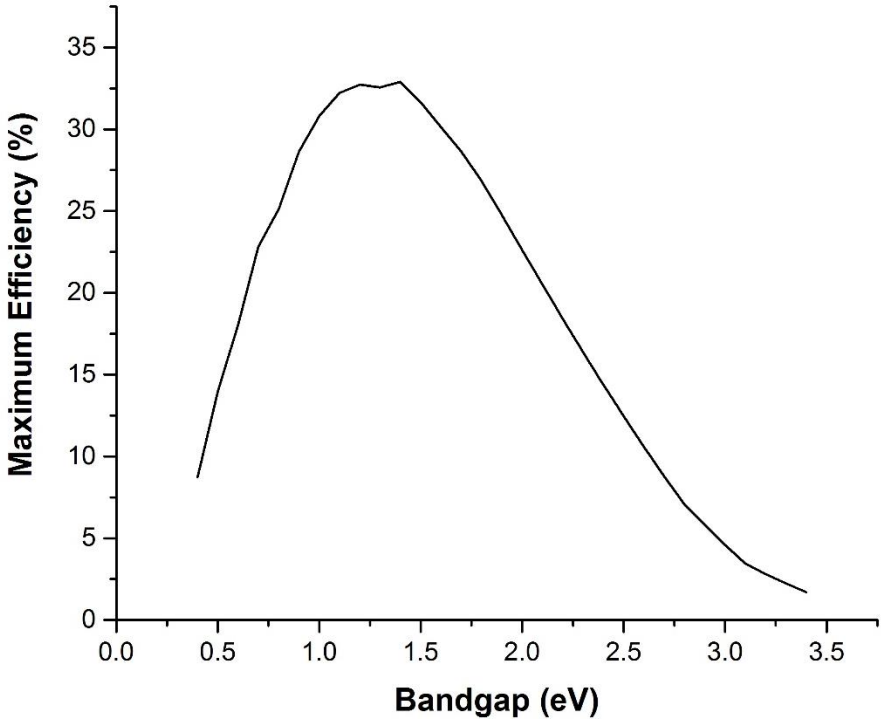

Figure 2.1: The Shockley-Queisser limit for the efficiency of a single-junction solar cell under unconcentrated sunlight.

Solar cells developments have always aimed at improving the power conversion efficiency and reducing manufacturing costs. Most of the solar cells produced are crystalline silicon which roughly accounts for 90% of the market [5]. The efficiency of the solar panels offered in today's market has reached up to 22%, with the majority still between 14% to 16% due to the high cost associated with making a highly efficient solar panels. It is important to note that most of the remaining solar energy that is not converted into electricity will be converted into heat inside the solar cells [6]. This increase in the solar cell temperature will have a negative affect the solar cell's power conversion efficiency and will reduces its lifetime damage the cell or possibly damage it. Therefore,

controlling the solar cell temperature by eliminating unwanted heat is of major importance and much research has focused on thermally managing the solar cells. The addition of a passively-cooled heat sink to the solar cell can reduce the solar cell's temperature by up to 15°C, which in turn can increase the affected power output by almost 7% [7]. One limiting factor of heat transferring between the solar cell and the heat sink is the interfacial thermal resistance between the two surfaces [8]. This is caused by microscopic imperfections of the two adjoined surfaces that will cause tiny air gaps between them. Since air is known to be a very poor thermal conductor, a good solution would be to fill these air gaps with a material that has much higher thermal conductivity [9]. This material, or paste, is referred to as Thermal Interface Material, or TIM. Several commercial TIMs are available in the market and the aim of the bulk of this research is to improve the thermal conductivity of those TIMs using better fillers like graphene [10-20].

1.2 Solar Irradiance and Air Mass

The sun has a blackbody surface temperature of 5777 K as first observed by Planck in 1901 [21]. Solar irradiance is the amount of power received from the sun by earth. This energy is measured in watt per square meter (W/m^2). This power is measured perpendicular to incident light and can be measured either in space or on earth. The solar irradiance reaching earth's outer atmosphere is around 1360 W/m^2 [22]. Once it enters the atmosphere, it loses some of the power due to scattering of light in earth's atmosphere and an average of about 1000 W/m^2 of solar irradiance reaches the surface of earth at sea level on a clear day. This value is also referred to as 1 sun. Air mass is used to characterize the

effects of atmosphere on the solar spectra and is defined as the relative length of direct beam travelling through the atmosphere compared to the vertical path to the sea level, as seen in Figure 1.2. As the sun moves away from the zenith angle, the light travels through greater lengths of the atmosphere and thus losing more energy before reaching the same point. Air Mass is expressed as AM=1/Cos(θ), so AM1.5 is obtained from 1/Cos(48.2°) = 1.5 as shown in Figure 2.3 [23]. The solar radiation at one point in earth is collected in several ways. The first is the direct radiation, which is the radiation reaching the collector directly and not reflected or scattered by the atmosphere. The second is the diffuse radiation which is the scattered radiation from atmosphere reaching the collector. The third is the ground radiation which is the radiation reflected from the ground and into the collector. All three radiations are referred to as global radiation AM1.5G and their total measured irradiance is 1000 W/m^2 or 1 sun, and the direct irradiance, AM1.5D is has only 768 W/m^2 irradiance.

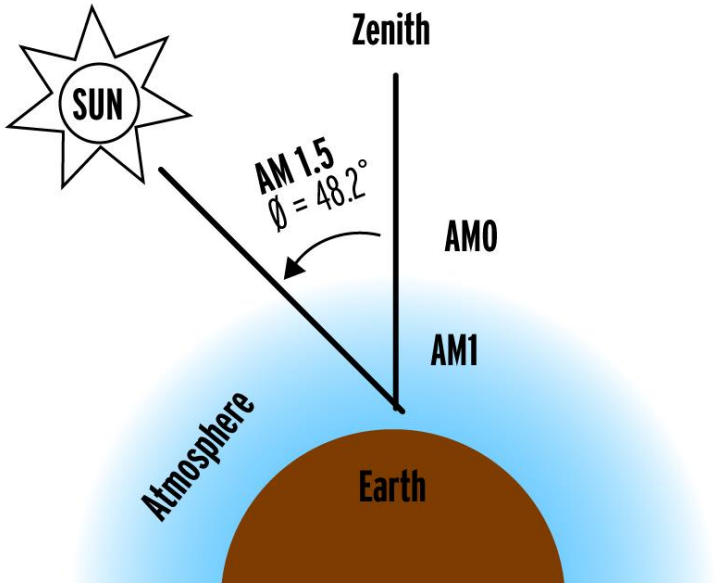

Figure 2.2: Air mass with the zenith angle.

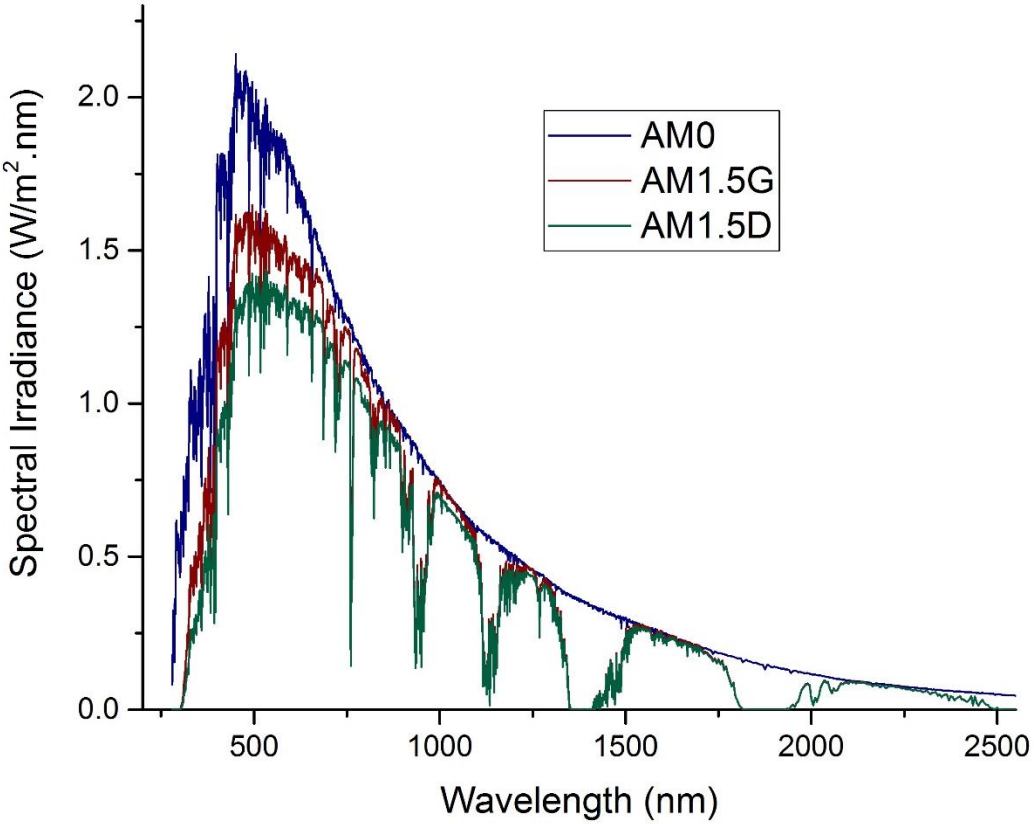

Figure 2.3: Solar spectra: AM0, AM1.5G, and AM1.5D.

1.3 Principles of Photovoltaic Solar Cells

A photovoltaic cell is a semiconductor that generates electric power directly from sunlight through a phenomenon called the photovoltaic effect. This phenomenon was first observed in electrolytes in 1839 by Becquerel, and in 1883 Fritts made the first PV device using Selenium film. The current design of solar cell was first made in Bell Labs in 1954 with an efficiency of only 6%. A conventional solar cell is formed by joining p-type material with a n-type material. The p-type and n-type materials are made by injecting impurities through a process called doping, n-type gets injected with donors and p-type gets injected with acceptors. The thickness of the p-type material is 300 μm compared to the thin layer of n-type which is 1 μm only as seen in Figure 1.4. The junction, where the p-type meets the n-type, has a bandgap energy E_g. At equilibrium, that energy is equal to the difference between the upper edge of the valence band and the lower edge of the conduction band. Incident light on PV cell is made of a beam of photons with energy $E = hv$, where h is Planck's constant and v is the frequency of the photon. If this energy equals to or more than the semiconductor's bandgap E_g, the photon is absorbed by the cell and an electron-hole pair is generated. This process of creating free electrons and holes carriers is referred to as photogeneration. The built in potential of the p-n junction causes the generated electrons to drift to the n-type region towards the external contact, and the generated holes move to the p-type region towards the p-side external contact. The accumulation of electrons and holes at the external contacts will generate a potential difference that will drive current through an external load.

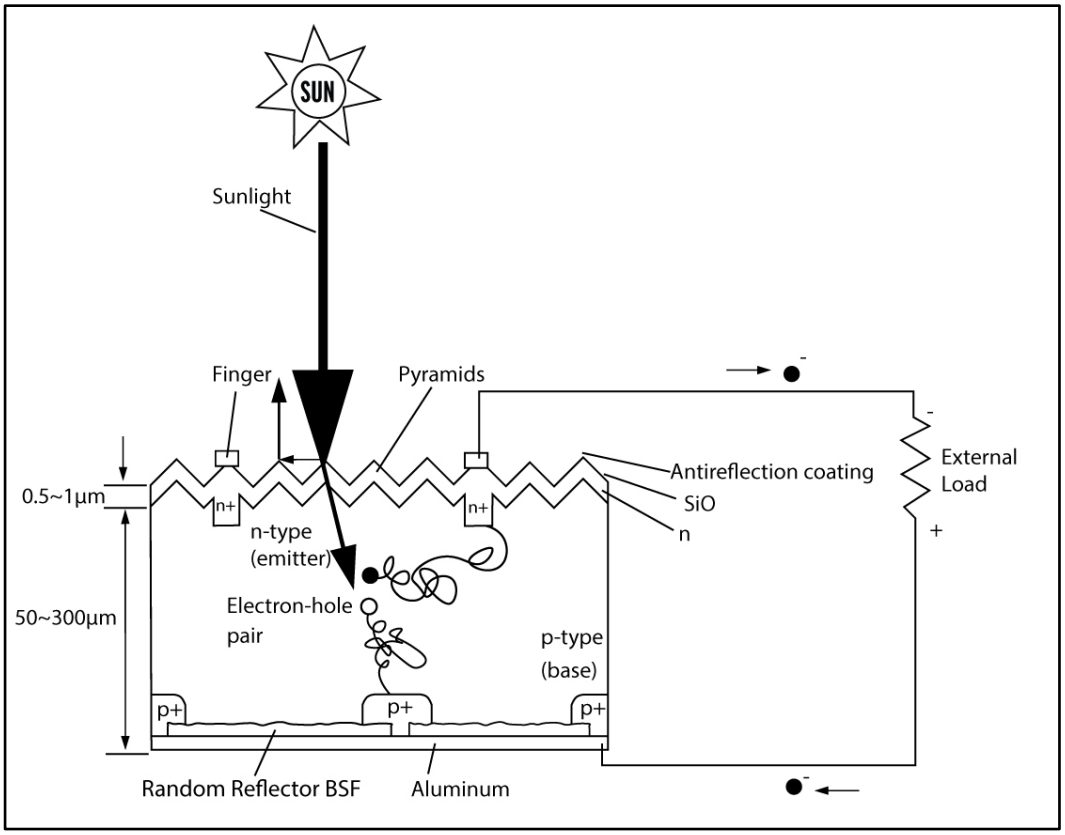

Figure 2.4 Schematic that illustrates the operation of a conventional solar cell.

There are two important parameters of photovoltaic cells. The first is the open-circuit voltage (V_{OC}) and it's the voltage between the two metal terminals of an illuminated photovoltaic cell with no load connected to them and zero current is flowing. The second parameter is called the short-circuit current (I_{sc}) and it is described as the maximum current flowing when the two external contacts are shorted together and having a zero voltage. The short-circuit current would then determine the rate of photogenerated electron-hole pairs.

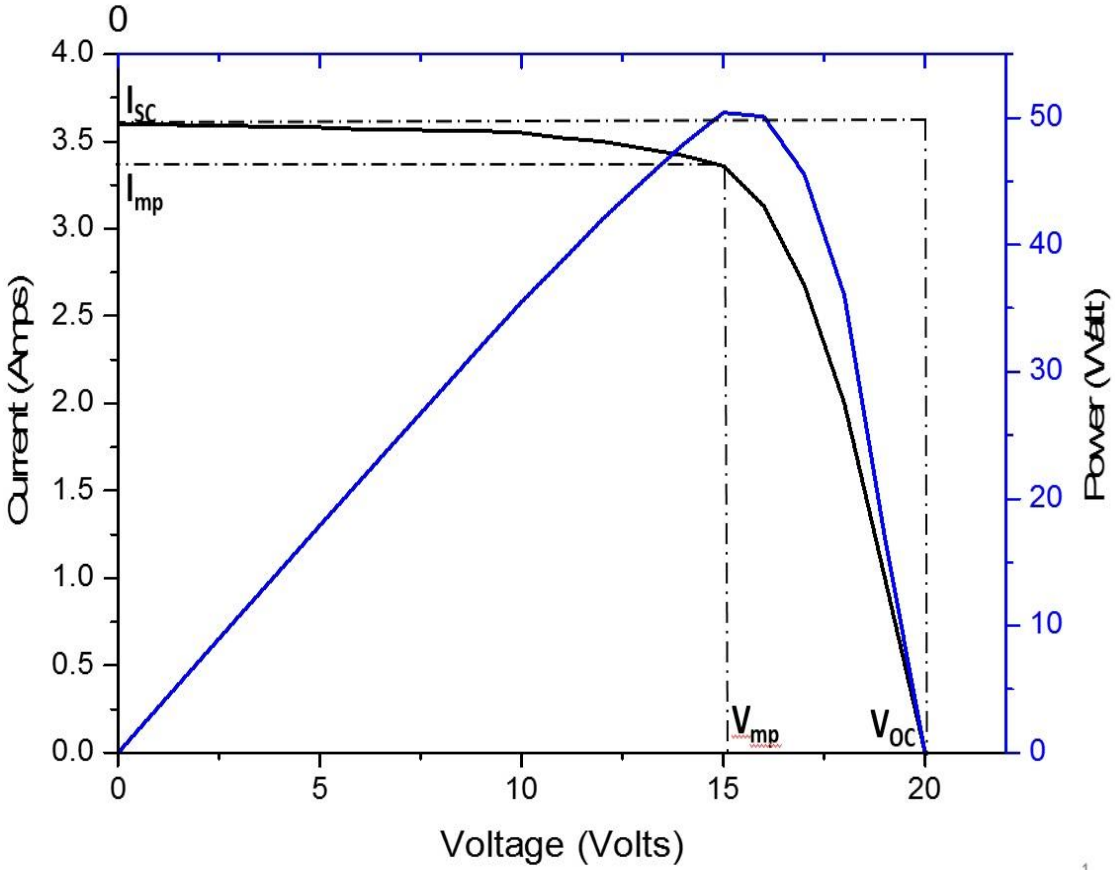

Figure 2.5: Current-voltage characteristics of a photovoltaic cell.

When connecting a resistive load, the current will be less than the short-circuit current I_{sc}. The voltage will also be less than the open-circuit voltage V_{OC}. The cell output power is given by:

$$P = IV, \tag{1.1}$$

where the following conditions are always valid:

$$I < I_{SC} \quad \text{and} \quad V < V_{OC} \tag{1.2}$$

The maximum power conditions can be found by deriving equation (1.1) and equating it to zero:

$$dP = d(IV) = IdV + VdI = 0 \quad (1.3)$$

The maximum power output is found at:

$$P_{mp} = I_{mp}V_{mp} \quad (1.4)$$

Figure 2.5 is the IV plot of a PV cell showing all I_{SC}, V_{OC}, P_{mp}, I_{mp}, and V_{mp}.

The fill factor of a solar cell *FF* is a parameter used to evaluate the quality of the current-voltage curve, and it can be described as the ration of the two rectangles in Figure 2.5. It is given by[24]:

$$FF = \frac{P_{mp}}{I_{sc}V_{oc}} = \frac{I_{mp}V_{mp}}{I_{sc}V_{oc}} \quad , \quad (1.5)$$

which has typical value of 0.8 to 0.9 for an efficient solar cell.

The most important parameter in solar cells is the power conversion efficiency, η which is the ratio of the solar cell output power to the incident light power entering the cell.

$$\eta = \frac{P_{mp}}{P_{in}} = \frac{FF.I_{sc}V_{oc}}{P_{in}} \quad (1.6)$$

Silicon solar cells usually have efficiencies (η) 15-21% [25] and multi-junction solar cells can have efficiencies up to almost 45% [26].

1.4 Types of Solar Cells

Solar cells can be classified based on the semiconductor material like crystalline silicon and the number of junctions like single-junction or multi-junction solar cells. The following subsections lists major types and their features.

1.4.1 Crystalline Silicon Solar Cells

The most common type of photovoltaic cell in production. This type of solar cells is made of the crystalline form of silicon and they can be either multicrystalline silicon or monocrystalline silicon. The monocrystalline silicon material has the same crystal structure throughout and the same orientation, whereas the multicrystalline silicon material is comprised of many small silicon grains in different orientations. The monocrystalline silicon is usually more expensive to manufacture than the multicryatalline silicon and have higher efficiencies.

1.4.2 Thin-Film Solar Cells

This type of solar cells is made of one or more thin layer of photovoltaic material on a substrate like metal or plastic. The thickness of thin-film is usually in nanometer to several micrometers compared to the crystalline silicon thickness of several hundreds of micrometers. Thin-film solar cells are usually cheaper and more flexible than conventional solar cells but have less efficiencies [27].

1.4.3 Organic Solar Cells

This type of PV solar cell is made of organic material like polymer solar cells. They can have a single layer or bilayer junction. They are cheaper to make than conventional solar cells and more environmentally friendly, but their efficiencies are much lower [28].

1.4.4 Multi-Junction Solar Cells

Multi-junction solar cells (MJ) have multiple p-n junctions made of different semiconductor materials. To describe it simply, the multi-junction solar cell can be described as several single junction solar cells on top of each other. These junctions allow the PV cell to have more than one bandgap and therefore a higher percentage of absorbed photons wavelengths which increases the overall efficiency of the solar cell. The limiting factor of MJ solar cells is that they're more expensive to manufacture than single-junction solar cells but perform much better under concentrated solar light. Their high efficiency compared to their small size make them useful for use in outer space [29].

1.4 Effects of Temperature on Efficiency

Photons incident on a solar cell have different wavelengths. Photons with long wavelength will penetrate into the p-type region and photons with shorter wavelength are mostly absorbed in the n-type region. Photons with energy below the solar cell's bandgap energy E_g do not contribute to the photogeneration process and their absorbed energies will produce phonons that convert to heat. Photons with energy above the bandgap energy will generate a photocurrent. The remaining energy above the bandgap will convert to kinetic energy that will also generate heat. This heat has a negative effect on the solar cell's performance.

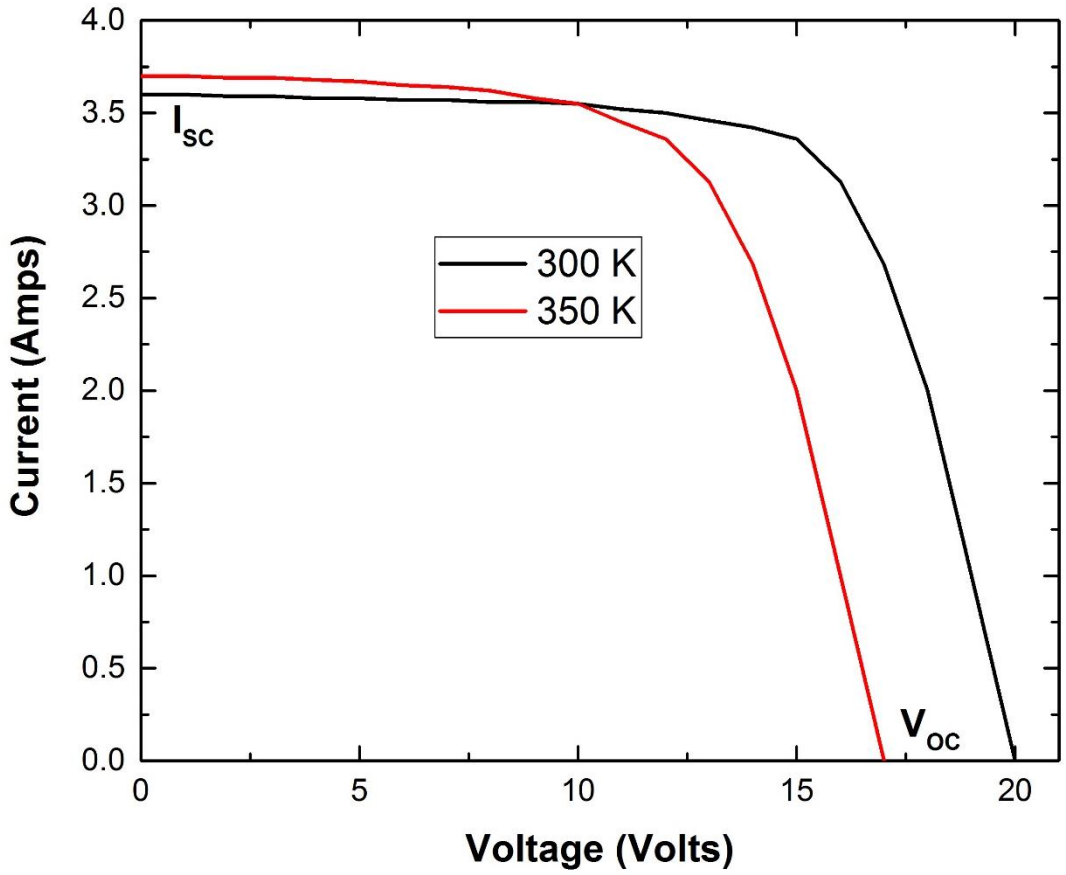

Figure 2.6: Temperature effects on the open circuit voltage (V_{OC}) and short circuit current (I_{SC}).

An increase in the solar cell temperature will cause a decrease in the bandgap energy, which will allow more photons to be absorbed. This increase in absorption will slightly increase the short-circuit current. Furthermore, a rise in the solar cell's temperature will have a negative impact on the open-circuit voltage and the fill factor which will eventually reduce the cell's efficiency Figure 2.6. Ref [30] reports that the output power of Si PV cell decreases 0.47%/°C. Experimental measurements of temperature effects on crystalline silicon solar cell showed that with increased operating temperature, a decrease of 0.65%/K

in the PV cell output power, a fill factor decrease of 0.2%/K, and a conversion efficiency decrease of 0.08%/K [31].

Solar cells can undergo long-term degradation if operating temperature exceeds certain limits [32]. The temperature degradation coefficient is usually given by the solar cell's manufacturer along with its maximum operating temperature. It is important to control the solar cell's temperature by removing of excess heat. Different techniques of cooling solar cells have been introduced, and the next section briefly explores them.

1.5 Thermal Managements of Solar Cells

Only a fraction of absorbed solar radiation energy is turned into useful output. The rest is converted to heat inside the cell. This heat is removed by two main approaches, passive cooling and active cooling [33].

1.5.1 Passive Cooling

Passive cooling is the removal of heat by flowing medium like air or water. Most solar cells uses passive cooling because of its reliability and low cost. Examples of passive cooling include heat sinks, heat pipes, and micro-channels. A heat sink is a metal device that absorbs the heat from the solar cell and dissipates it into the surrounding air by natural or forced heat convection. Heat sinks are made of materials with high thermal conductivity like aluminum or copper. They can be shaped as a flat panel below a solar cells array with fin arrays in one side, or many sides if the design allows or using single solar cell. Natural

conviction occurs when cooling air flows normally through the fin array, whereas forced conviction is when air flow is forced by the use of a fan. Forced cooling provides a more cooling than natural cooling but requires additional power to operate the fan. Natural cooling is preferred for solar cells as it is easier to implement and cost less. Heat sinks are optimized by changing the geometrical shape of the fins. Water can also be used to cool heat sinks. In this case, more heat exchange takes place due to the higher heat capacity of water. Output power of a forced air cooling PV cell increased by 10% over natural air cooling and 66% with water cooling [34].

Heat pipes are another method of passively cooling solar cells [35]. Heat pipes are metal pipes filled with small amount of water that transfers heat by evaporating and condensing in continuous cycles. They require no input power and can effectively transfer heat over a long distance. When heat is absorbed at one end of the pipe, it causes water to evaporate. The increasing vapor pressure results in a difference in pressure which drives the vapor to the other end of the heat pipe, the condenser section, which is placed in a cooler environment. The section between the hot and cold ends is the transfer section where two states of the liquid flow in opposite directions. Heat pipe cooling is a suitable option for solar cells under concentrated conditions due to its excellent thermal conductivity and constant temperature uniformity. Fins can be utilized at the condenser section to increase heat exchange. Microchannel cooling is another form of passive cooling that can transfer large amount of heat from a small area. A rectangular channel made of high thermal conductivity material where inner fluid thermal conductivity is inversely proportional to the channel width.

1.5.2 Active Cooling

Active cooling is done by collecting heat from the solar cell and using it in other useful applications such as water heating. This technique is also referred to as photovoltaic/thermal collector, PV/T, and it utilizes both electrical and heat energies of the system.

1.6 Cooling Compounds

There are several two main types of compounds used to absorb or dissipate the heat out of electronic devices, Thermal interface materials and Phase Change Materials (PCM). We will go through each of them briefly in the following subsections.

1.6.1 Thermal Interface Materials

Thermal interface materials (TIMs) are used to enhance the thermal conductance between two contacting surfaces [36-39]. When two adjoining surfaces such as the solar cell back panel and a heat panel are joined together to transfer heat, air gaps caused by defects in the two surfaces can cause thermal contact resistance between the two surfaces. Thermal interface materials, generally in the form of paste, is used to fill these air gaps and provide a better thermal contact between the two surfaces.

Thermal interface material performance depends on its thermal conductivity. The higher thermal conductivity for the TIM the better thermal contact between the two surfaces. While TIMs provide better thermal conductance than air, they are less heat

conducting than heat conducting metals like aluminum or copper. TIMs are made of composite materials with metallic or ceramic fillers that enhances thermal conductivity. Solid metallic particles like aluminum or silver provide a better thermal conductance and when ceramic particles are used when electrical insulation is required. Thermal interface materials must also be designed to spread effectively under surfaces pressure. A TIM that has a better spreading characteristics can enhance the interfacial thermal contact by eliminating more air pockets between the two surfaces.

Another important feature to consider in choosing thermal interface materials is its durability. Performance stability and reliability of TIMs over long operating times is important and TIMs with higher viscosities are used for this. It is crucial to apply TIMs appropriately. Excess amounts can have negative results and amounts that are too low can result smaller spreading than required. The TIM must also be easily removed when replacement is required. Other factors to consider in TIMs include cost and corrosion resistance. Fillers made from silver or graphene provides excellent thermal conductivities but cost much more that other fillers like aluminum. Additionally, TIMs must not cause long time corrosions to surfaces where they have been applied. A typical use of thermal interface material (TIM) can be seen in Figure 2.7 where it is applied between two surfaces, the back surface of a heat generating source, a solar cell in this case, and the surface of a heat sink or heat spreader. A zoomed in view of the surfaces contacts reveals the microscopic surfaces imperfections caused by the surfaces roughness and the air gaps that are filled with the interface material.

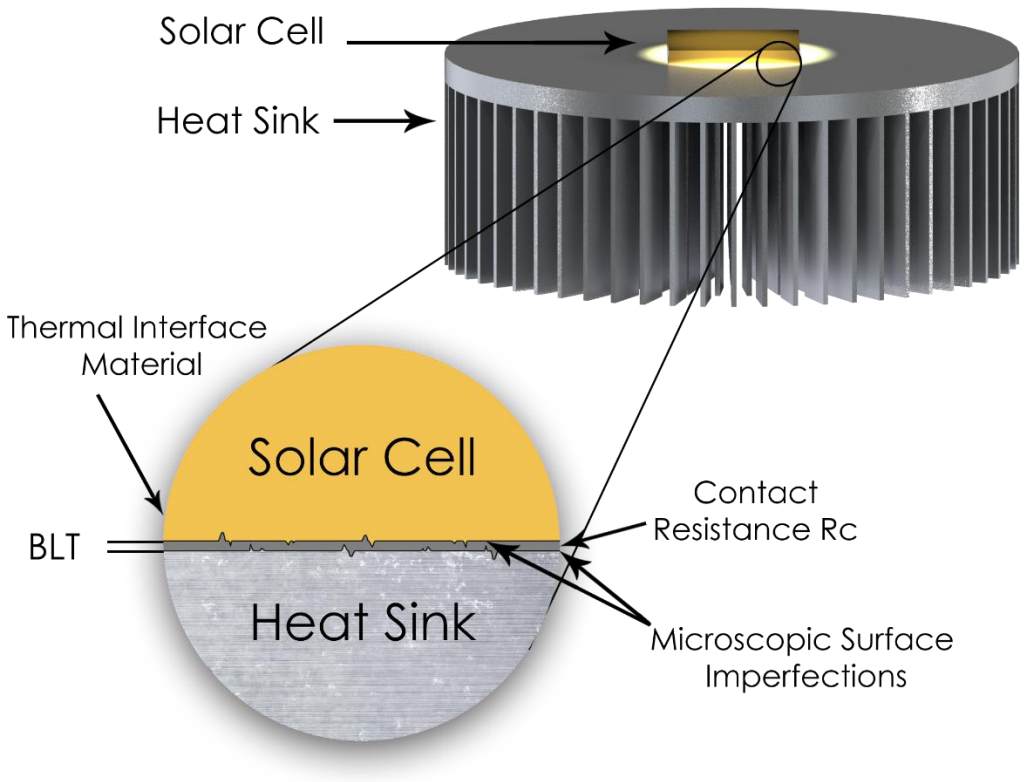

Figure 2.7: Thermal interface material used to fill the gaps between the two surfaces.

The distance between the two surfaces is called the bond-line thickness (BLT) and the contact resistances between TIM and the two surfaces, R_{C1} and R_{C2}, are used to calculate the TIM effective thermal resistance, R_{TIM}:

$$R_{TIM} = \frac{BLT}{K_{TIM}} + R_{C1} + R_{C2} \tag{1.7}$$

where K_{TIM} is the thermal conductivity of the TIM [36].

1.6.2 Phase Change Materials

Phase change materials work differently than thermal interface materials. While thermal interface material helps the thermal conductivity between two surfaces, the phase change material absorbs the heat by itself. The PCM is made of a material with a high heat of fusion. It will continue to absorb or release heat until the material is completely change from the solid phase to a liquid phase or vice versa as shown in Figure 2.8. The temperature point where the material starts absorbing and changing its phase is called the melting point. The melting point is important and varies according to the desired application needs. For example, a typical solar panel which reaches a temperature of 80° C in peak operation will require a phase change material with a melting point of 80° C to maximize the benefit.

Phase change material have advantages and disadvantages when compared to thermal interface materials. Their main advantage is that they're cheaper than thermal interfsace material. They are also more environmentally friendly, non-toxic, and non-corrosive. They have a higher number of operating cycles and more durable than Thermal interface materials. Their main disadvantage however will outweigh all their advantages, and it is that they can eliminate less overall heat than a thermal interface material. While they might be a good solution to use with solar panels, they are not as practical at all to use with small, high heat electronics like computer processors as thermal interface materials with dissipating heat sinks.

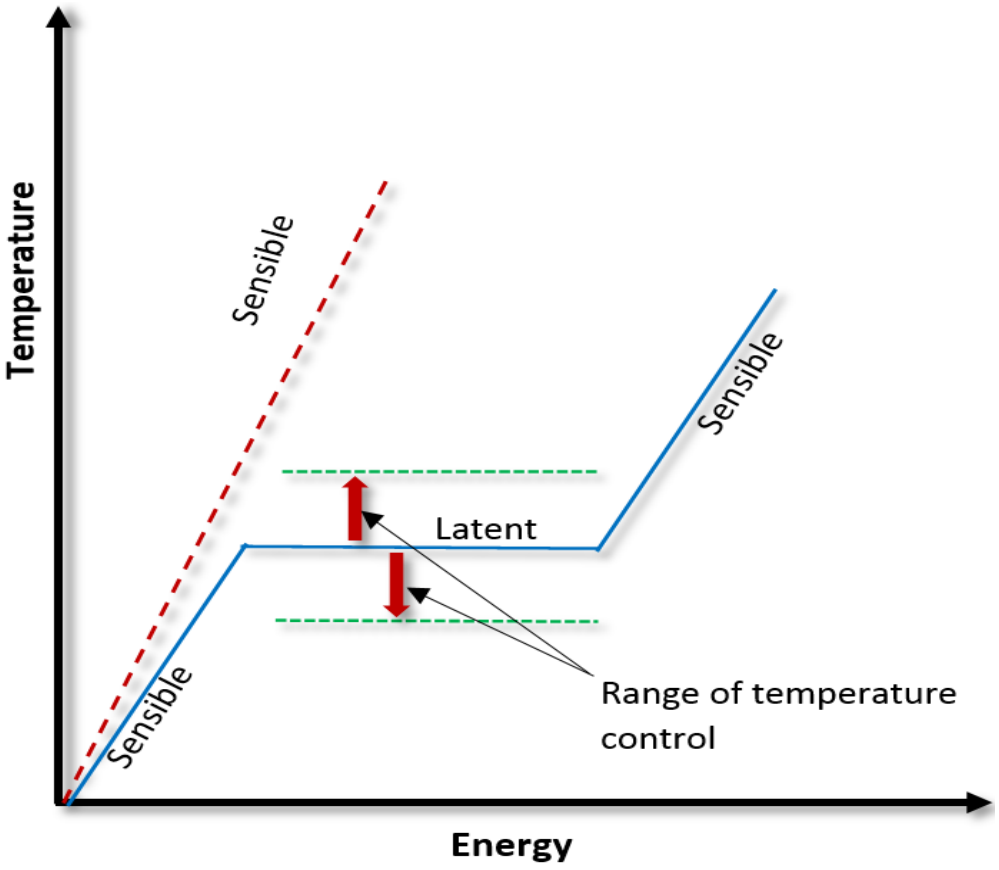

Figure 2.8: The basic operation of the phase change material (PCM).

1.7 Graphene

Graphene is a sheet of single-layered carbon atoms packed densely into a honeycomb crystal lattice [40]. Prior to its discovery in 2004, suspended graphene was not considered to exist in a free state [41]. Graphene is characterized by its high intrinsic thermal conductivity ranging from 3-5.3 KW/m K, high electron mobility, and low resistivity [42-44]. The superior thermal and electrical properties of graphene make it an excellent material for thermal management, low noise transistors, and electrical interconnects.

1.6.1 Graphene to Improve Thermal Conductivity of TIMs

The ongoing decrease in electronics size and increase in its power density have raised the demand for better thermal management and heat dissipation [45]. The development of an improved thermal interface material with higher thermal dissipation crucial to the thermal management of next generation electronics. Conventional TIMs are generally made of polymeric or grease base material loaded with conductive materials like silver particles at high loading volume fractions f reaching up to 70% [46]. The increase in loading fraction f can negatively affect the TIM performance and increase its cost. Several attempts have been made to develop a hybrid graphene-metal based thermal interface materials with a reduced loading fraction f [47]. A report of 500% increase in thermal conductivity of the TIM was observed with the addition of small graphene volume loading fraction of $f \sim 5\%$. This significant improvement in the TIM thermal conductivity is largely owed by the superb intrinsic thermal conductivity of graphene and the strong graphene coupling to matrix materials.

References

[1] Chapin, Daryl M., C. S. Fuller, and G. L. Pearson. "A new silicon p-n junction photocell for converting solar radiation into electrical power." *Journal of Applied Physics* 25, no. 5 (1954): 676-677.

[2] Shockley, William, Hans Queisser, and Hans J Queisser. 1961. “The Shockley-Queisser Limit.” *Journal of Applied Physics* 32: 510–19.

[3] Lee, Ho Sung. *Thermal design: heat sinks, thermoelectrics, heat pipes, compact heat exchangers, and solar cells*. John Wiley & Sons, 2010.

[4] Europe, Solar Power. "Global market outlook for solar power 2015–2019." *Euoropean Photovoltaic Industry Association, Bruxelles, Tech. Rep* (2015).

[5] Saga, Tatsuo. 2010. “Advances in Crystalline Silicon Solar Cell Technology for Industrial Mass Production.” *NPG Asia Materials* 2 (3): 96–102. doi:10.1038/asiamat.2010.82.

[6] Green, Martin A., Keith Emery, Yoshihiro Hishikawa, Wilhelm Warta, and Ewan D. Dunlop. 2016. “Solar Cell Efficiency Tables (Version 47).” *Progress in Photovoltaics: Research and Applications*. doi:10.1002/pip.2728.

[7] Bojanampati, Shrinivas, Peter Rodgers, and Valerie Eveloy. "Experimental assessment of flat-type photovoltaic module thermal behavior." In *Thermal, Mechanical and Multi-Physics Simulation and Experiments in Microelectronics and Microsystems (EuroSimE), 2012 13th International Conference on*, pp. 1-4. IEEE, 2012.

[8] Gwinn, J. P., and R. L. Webb. 2003. “Performance and Testing of Thermal Interface Materials.” In *Microelectronics Journal*, 34:215–22. doi:10.1016/S0026-2692(02)00191-X.

[9] Prasher, R. 2006. “Thermal Interface Materials: Historical Perspective, Status, and Future Directions.” *Proceedings of the IEEE* 94 (8): 1571–86. doi:10.1109/JPROC.2006.879796.

[10] Renteria, Jackie D., Denis L. Nika, and Alexander A. Balandin. "Graphene thermal properties: applications in thermal management and energy storage." *Applied Sciences* 4, no. 4 (2014): 525-547.

[11] Goli, Pradyumna, Stanislav Legedza, Aditya Dhar, Ruben Salgado, Jacqueline Renteria, and Alexander A. Balandin. "Graphene-enhanced hybrid phase change materials for thermal management of Li-ion batteries." *Journal of Power Sources* 248 (2014): 37-43.

[12] Yan, Zhong, Denis L. Nika, and Alexander A. Balandin. "Thermal properties of graphene and few-layer graphene: applications in electronics." *IET Circuits, Devices & Systems* 9, no. 1 (2015): 4-12.

[13] Malekpour, H., K-H. Chang, J-C. Chen, C-Y. Lu, D. L. Nika, K. S. Novoselov, and A. A. Balandin. "Thermal conductivity of graphene laminate." *Nano Letters* 14, no. 9 (2014): 5155-5161.

[14] Renteria, J., S. Legedza, R. Salgado, M. P. Balandin, S. Ramirez, M. Saadah, F. Kargar, and A. A. Balandin. "Magnetically-functionalized self-aligning graphene fillers for high-efficiency thermal management applications." *Materials & Design* 88 (2015): 214-221.

[15] Khandelwal, Ratnesh, and JM Chandra Kishen. "Thermal weight functions for bi-material interface crack system using energy principles." *International Journal of Solids and Structures* 45, no. 24 (2008): 6157-6176.

[16] Memon, Muhammad Omar, Sylvain Haillot, and Khalid Lafdi. "Carbon nanofiber based buckypaper used as a thermal interface material." *Carbon* 49, no. 12 (2011): 3820-3828.

[17] Li, Xiaobo, and Ronggui Yang. "Effect of lattice mismatch on phonon transmission and interface thermal conductance across dissimilar material interfaces." *Physical Review B* 86, no. 5 (2012): 054305.

[18] Goyal, Vivek, and Alexander A. Balandin. "Thermal properties of the hybrid graphene-metal nano-micro-composites: Applications in thermal interface materials." *Applied Physics Letters* 100, no. 7 (2012): 073113.

[19] Sarvar, Farhad, David C. Whalley, and Paul P. Conway. "Thermal interface materials-A review of the state of the art." In *Electronics Systemintegration Technology Conference, 2006. 1st*, vol. 2, pp. 1292-1302. IEEE, 2006.

[20] Shahil, Khan MF, and Alexander A. Balandin. "Thermal properties of graphene and multilayer graphene: Applications in thermal interface materials." *Solid State Communications* 152, no. 15 (2012): 1331-1340.

[21] Planck, M. 1901. "On the Law of Distribution of Energy in the Normal Spectrum On the Law of Distribution of Energy in the Normal Spectrum." *Annalen Der Physik* 4 (3): 553–63. doi:10.1002/andp.19013090310.

[22] Gueymard, Christian A. 2004. "The Sun's Total and Spectral Irradiance for Solar Energy Applications and Solar Radiation Models." *Solar Energy* 76 (4): 423–53. doi:10.1016/j.solener.2003.08.039.

[23] ASTM International. ASTM G173-03(2012) Standard Tables for Reference Solar Spectral Irradiances: Direct Normal and Hemispherical on 37° Tilted Surface. West Conshohocken, PA: *ASTM International*, 2012. doi: https://doi.org/10.1520/G0173-03R12.

[24] Chen, C. Julian. *Physics of Solar Energy*. John Wiley & Sons, 2011.

[25] Green, Martin A., Keith Emery, Yoshihiro Hishikawa, Wilhelm Warta, and Ewan D. Dunlop. 2016. "Solar Cell Efficiency Tables (Version 47)." *Progress in Photovoltaics: Research and Applications*. doi:10.1002/pip.2728.

[26] Dimroth, Frank, Matthias Grave, Paul Beutel, Ulrich Fiedeler, Christian Karcher, Thomas N D Tibbits, Eduard Oliva, et al. 2014. "Wafer Bonded Four-Junction GaInP/GaAs//GaInAsP/GaInAs Concentrator Solar Cells with 44.7% Efficiency." *Progress in Photovoltaics: Research and Applications* 22 (3): 277–82. doi:10.1002/pip.2475.

[27] Green, Martin A. "Crystalline silicon solar cells." *Clean Electricity from Photovoltaics* 1 (2001): 149.

[28] Choy, Wallace CH, and W. All AceChik Ho. *Organic solar cells*. Vol. 2. London: Springer-Verlag, 2013.

[29] Yamaguchi, Masafumi, Tatsuya Takamoto, Kenji Araki, and Nicholas Ekins-Daukes. "Multi-junction III–V solar cells: current status and future potential." *Solar Energy* 79, no. 1 (2005): 78-85.

[30] Messenger, Roger, D. Yogi Goswami, Hari M. Upadhyaya, Takhir M. Razykov, Ayodhya N. Tiwari, Roland Winston, and Robert McConnell. "Photovoltaics Fundamentals, Technology and Application." In *Energy Conversion*, pp. 20-1. CRC Press, 2007.

[31] Radziemska, E. "The effect of temperature on the power drop in crystalline silicon solar cells." *Renewable Energy* 28, no. 1 (2003): 1-12.

[32] Royne, Anja, Christopher J. Dey, and David R. Mills. 2005. “Cooling of Photovoltaic Cells under Concentrated Illumination: A Critical Review.” *Solar Energy Materials and Solar Cells*. doi:10.1016/j.solmat.2004.09.003.

[33] Ye, Zhangbo, Qifen Li, Qunzhi Zhu, and Weiguo Pan. 2009. “The Cooling Technology of Solar Cells under Concentrated System.” In *2009 IEEE 6th International Power Electronics and Motion Control Conference, IPEMC ’09*, 2193–97. doi:10.1109/IPEMC.2009.5157766.

[34] Bojanampati, Shrinivas, Peter Rodgers, and Valerie Eveloy. "Experimental assessment of flat-type photovoltaic module thermal behavior." In *Thermal, Mechanical and Multi-Physics Simulation and Experiments in Microelectronics and Microsystems (EuroSimE), 2012 13th International Conference on*, pp. 1-4. IEEE, 2012.

[35] Farahat, M. A. "Improvement the thermal electric performance of a photovoltaic cells by cooling and concentration techniques." In *Universities Power Engineering Conference, 2004. UPEC 2004. 39th International*, vol. 2, pp. 623-628. IEEE, 2004.

[36] Tong, Xingcun Colin. *Advanced materials for thermal management of electronic packaging*. Vol. 30. Springer Science & Business Media, 2011.

[37] Khandelwal, Ratnesh, and JM Chandra Kishen. "Thermal weight functions for bi-material interface crack system using energy principles." *International Journal of Solids and Structures* 45, no. 24 (2008): 6157-6176.

[38] Memon, Muhammad Omar, Sylvain Haillot, and Khalid Lafdi. "Carbon nanofiber based buckypaper used as a thermal interface material." *Carbon* 49, no. 12 (2011): 3820-3828.

[39] Li, Xiaobo, and Ronggui Yang. "Effect of lattice mismatch on phonon transmission and interface thermal conductance across dissimilar material interfaces." *Physical Review B* 86, no. 5 (2012): 054305.

[40] Ferrari, Andrea C., J. C. Meyer, V. Scardaci, C. Casiraghi, Michele Lazzeri, Francesco Mauri, S. Piscanec et al. "Raman spectrum of graphene and graphene layers." *Physical review letters* 97, no. 18 (2006): 187401.

[41] Novoselov, Kostya S., Andre K. Geim, Sergei V. Morozov, D. Jiang, Y_ Zhang, Sergey V. Dubonos, Irina V. Grigorieva, and Alexandr A. Firsov. "Electric field effect in atomically thin carbon films." *science* 306, no. 5696 (2004): 666-669.

[42] Balandin, Alexander A., Suchismita Ghosh, Wenzhong Bao, Irene Calizo, Desalegne Teweldebrhan, Feng Miao, and Chun Ning Lau. "Superior thermal conductivity of single-layer graphene." *Nano letters* 8, no. 3 (2008): 902-907.

[43] Konatham, D., D. V. Papavassiliou, and A. Striolo. "Thermal boundary resistance at the graphene–graphene interface estimated by molecular dynamics simulations." *Chemical Physics Letters* 527 (2012): 47-50.

[44] Alofi, A., and G. P. Srivastava. "Thermal conductivity of graphene and graphite." *Physical Review B* 87, no. 11 (2013): 115421.

[45] Goyal, Vivek, and Alexander A. Balandin. "Thermal properties of the hybrid graphene-metal nano-micro-composites: Applications in thermal interface materials." *Applied Physics Letters* 100, no. 7 (2012): 073113.

[46] Shahil, Khan MF, and Alexander A. Balandin. "Thermal properties of graphene and multilayer graphene: Applications in thermal interface materials." *Solid State Communications* 152, no. 15 (2012): 1331-1340.

[47] Shahil, Khan MF, and Alexander A. Balandin. "Graphene–multilayer graphene nanocomposites as highly efficient thermal interface materials." *Nano Letters* 12, no. 2 (2012): 861-867.

Chapter 2

Experiment Setup

This chapter describes the instruments used and the methodology of preparing and testing TIMs compounds on solar cells.

2.1 Equipment Used

Many instruments have been used in this research. The main ones are two solar simulators, one built in house and the other a professional high-end simulator bought from Newport Corporation. The other two instruments are used to measure thermal conductivity where one uses hot/cold disks to measure temperature gradient and the other uses xenon lamp to heat samples in-plane and cross-plane and records the temperature change. Following is a detailed description of each of these instruments.

2.1.1 Solar Simulator

Solar cells simulation module which consists of a 600W high pressure sodium bulb that produces light intensity of 85,000 lumens and 2,100 K color temperature, two solar

cells each with a heat sinks attached to it. The heat sinks are screwed to the solar cells where the solar cells are inside the enclosure and the heat sinks are outside. Between them is the enclosure chassis with an opening so that the solar cell's back is touching the heat sink. This is where the thermal interface material is applied. The setup of this experiment is demonstrated in Figure 2.1.

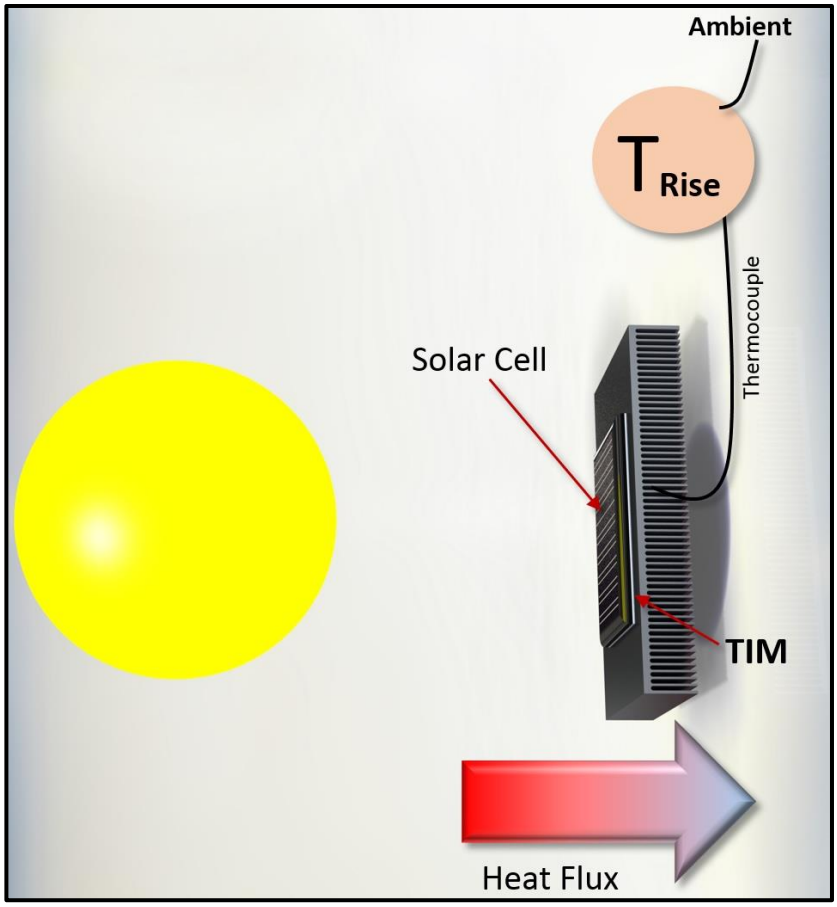

Figure 2.1: Schematic of the solar cells module.

A precision electronic weight balance is used to measure the thermal interface materials and graphene to be mixed [1]. Then a magnetic stirrer is used to mix the thermal paste with the graphene nano-powder and a power screw driver with adjustable torque

settings. This device insures that having the same torque setting when securing the solar cell to the heat sink in all test trials. This subsequently provides a uniform pressure for the thermal interface material. A multi-channel temperature logger is used to log the heat sink and ambient temperatures every 10 seconds as shown in Figure 2.2 [2].

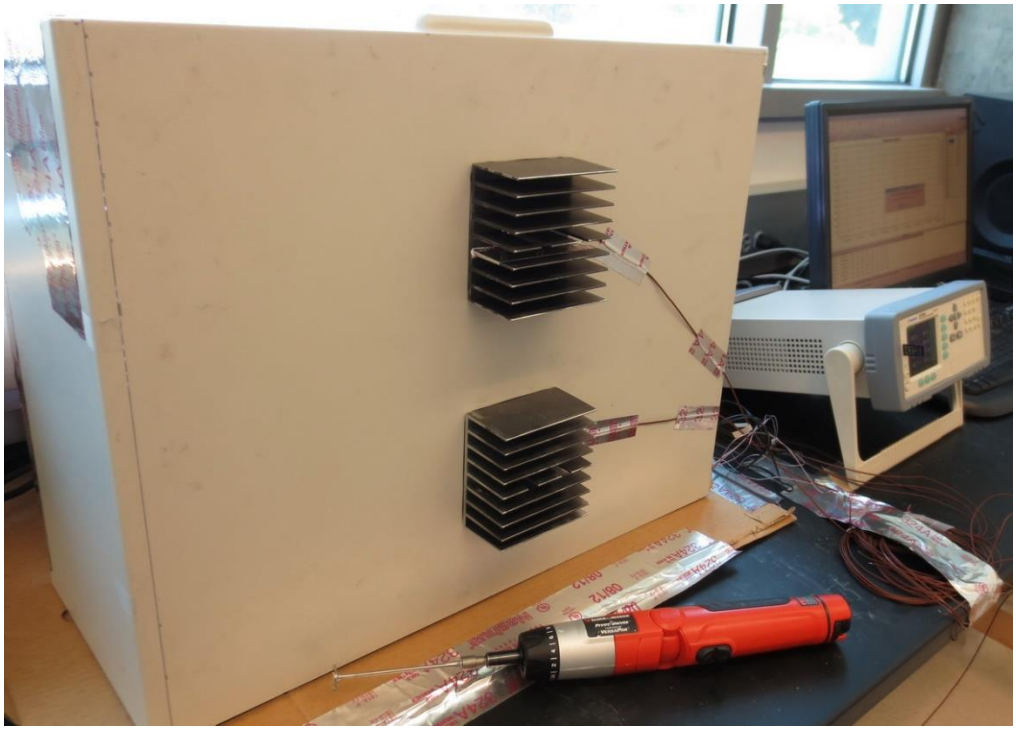

Figure 2.2: Image of the solar cells testing module.

2.1.2 Advanced Solar Simulator

The Oriel Sol1A class ABB solar simulator is a commercially made high performance solar simulator that utilizes a Xenon lamp that produces a 6”x6” beam size output that can be used for testing solar cells [3]. The image of the solar simulator can be seen in Figure 2.3.

Figure 2.3: Image of the Oriel Sol1A class ABB solar simulator.

This solar simulator emits a 5800K blackbody-like spectrum. This simulator obtains its power from a highly regulated power supply that insures a uniform level of illumination. The schematic of the solar simulator, Figure 2.4, illustrates the beam reflected from the Xenon lamp using a mirror then it passes through a spectral correction filter that simulates earth's AM1.5G solar spectra. A collimating lens is used to emulate the 0.5° angle of the sunlight reaching earth as seen in Figure 2.5. The power supply can be adjusted to produce a light concentration between 0.8 – 1.2 sun output.

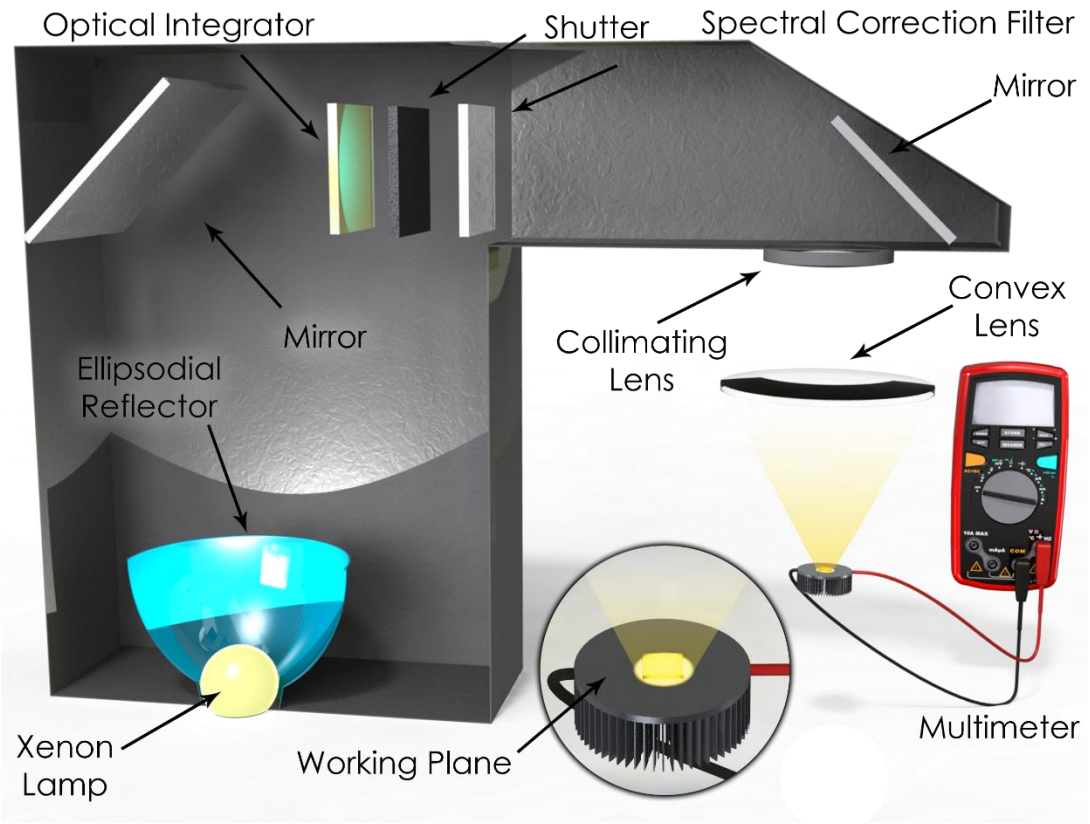

Figure 2.4: Schematic of the ABB solar simulator.

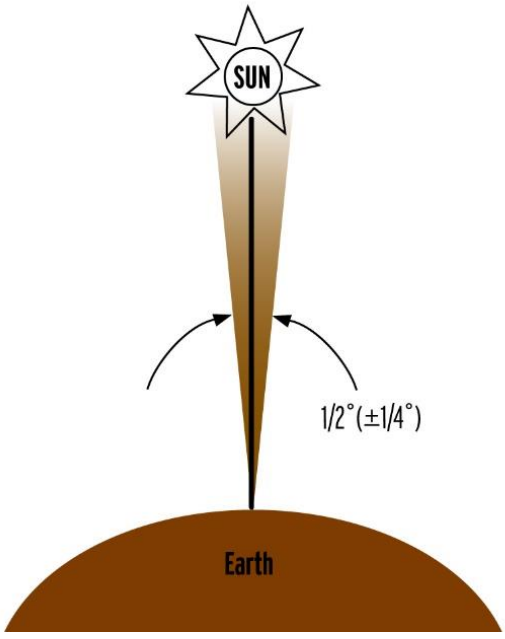

Figure 2.5: The solar disk subtends a 0.5° angle at the earth.

2.1.3 Thermal Interface Material Tester

The TIM Tester is an automated instrument that measures the thermal conductivity of thin layers of thermal interface materials and phase change materials (PCM), Figure 2.6. The sample is sandwiched between two surfaces conductive surfaces where one is heated and the other is cooled. The system allows the samples to be tested under varying pressure of 50-2600 kpa with the option of adjusting the sample temperature between 20°C and 130°C for thermal interface materials [4].

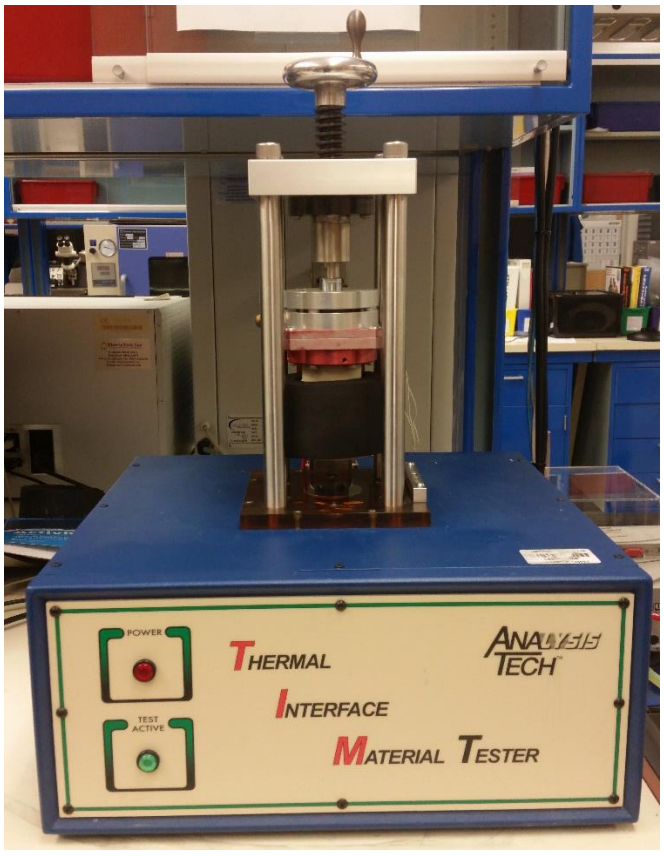

Figure 2.6: Thermal Interface Materials Tester image.

The instrument measures thermal conductivity k as:

$$k = \frac{Q.X}{(T_H - T_C).A},$$

where T_H, T_C are the two surfaces temperatures, A is the area of the sample, X is the sample's thickness, and Q is the steady state power. The thermal conductivity is also expressed as the reciprocal of the thermal resistivity R between the two parallel surfaces:

$$k = \frac{X}{R.A},$$

where,

$$R = \frac{T_H - T_C}{Q}$$

2.1.4 Laser Flash

The LFA 447 by Netzsch, Figure 2.7, is another instrument that measures the thermal conductivity, specific heat, and thermal diffusivity of different kinds of solid and liquid materials. The LFA 447 heat source is generated from a Xenon lamp [5]. The sample density and mass must be known to the user before testing it. Then the sample is coated with a thin layer of graphite so it can absorb as much heat as possible from the flash lamp heat source. The heat is subjected on the sample from one side and an IR detector measures temperature rise on the other side, Figure 2.8. Recorded data is then converted into a voltage signal that is plotted over time as shown in Figure 2.9.

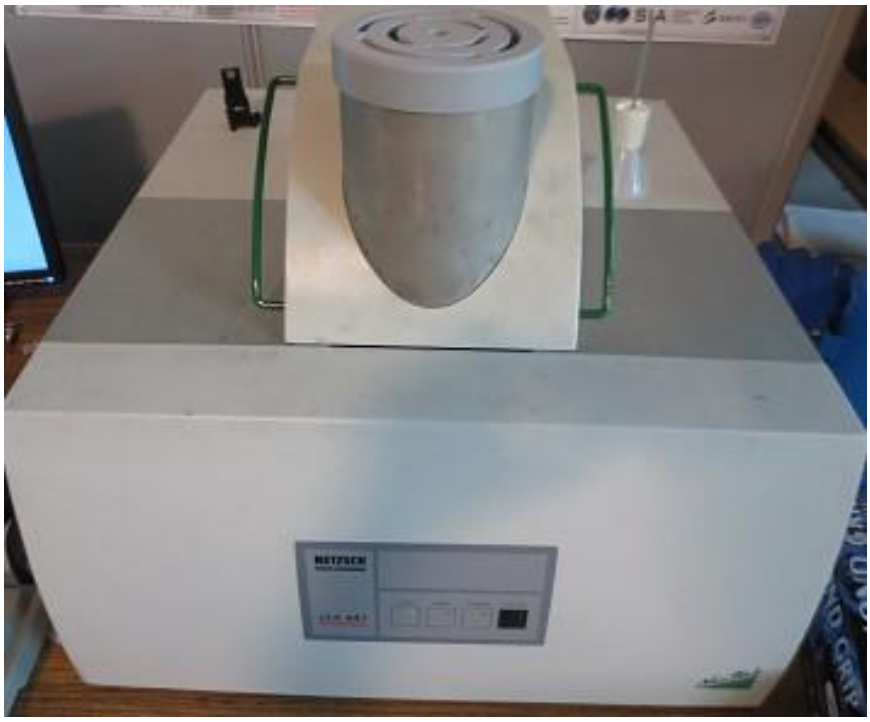

Figure 2.7: Image of LFA 447 Laser Flash instrument.

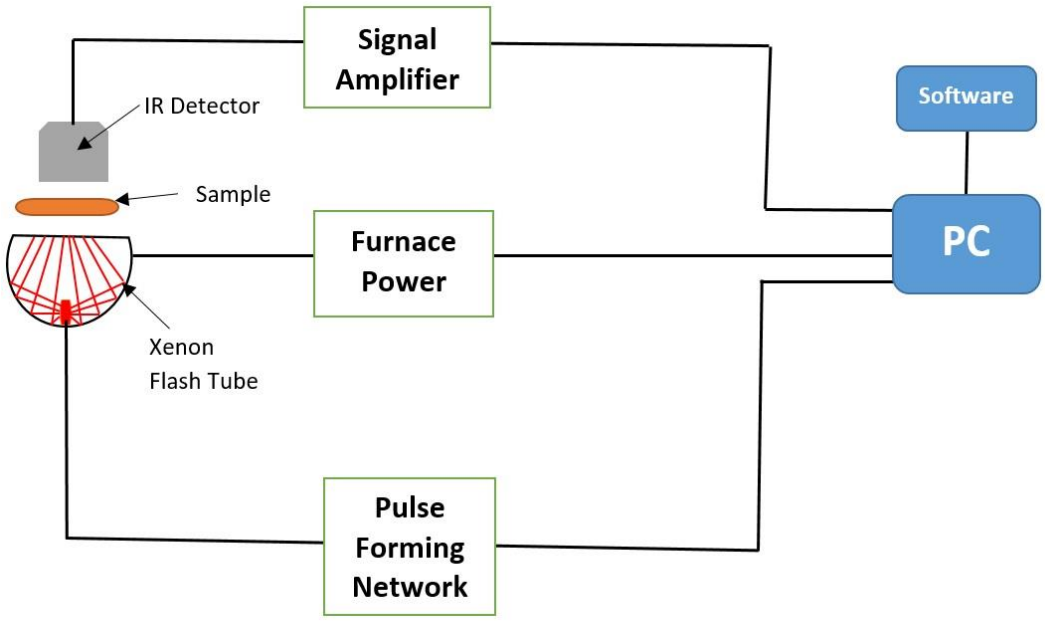

Figure 2.8: Laser Flash measurement principle.

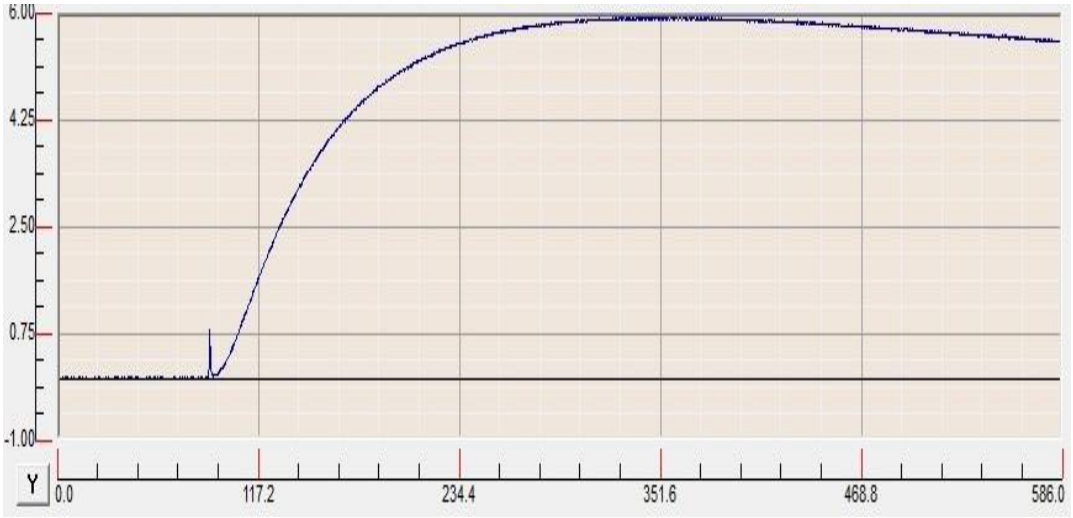

Figure 2.9: Laser Flash temperature over time output plot.

The system uses a Nano Flash software that utilizes specific approximations models to measure the thermal diffusivity of the sample. The most basic model is the adiabatic approximation and it calculates the thermal diffusivity *a* in (cm^2/s) by:

$$a = 0.1388 * \frac{l^2}{t_{50}},$$

where, *l* is the sample thickness (in cm), and t_{50} is the time (in seconds) taken to reach half its maximum temperature. The system also measures the specific heat *C* with the aid of a reference sample with known specific heat. The specific heat *C* is given by:

$$C = \frac{Q}{m\Delta T},$$

where *Q* is the energy, *m* is the sample mass, and ΔT is the change in sample's temperature. Since the energy *Q* is the same for both the sample and the reference, then:

$$Q_S = Q_R$$

Then

$$(mC\Delta T)_R = (mC\Delta T)_S$$

Which finally gives us:

$$C_s = \frac{(mC\Delta T)_R}{(m\Delta T)_S}$$

The thermal conductivity of the sample is ultimately given by:

$$\lambda(T) = a(T) \cdot \rho(T) \cdot c(T),$$

where, λ is the thermal conductivity, a is the thermal diffusivity, ρ is the bulk density, and c is the specific heat.

2.2 Materials Used

Three commercial thermal interface materials were used [6-9]. Their properties are listed in table 2.1

Table 2.1: Physical properties of top commercial thermal interface materials.

TIM	Filler Material	Density (g/cm^3)	Cure Time (Hrs.)
MX-4	Carbon	2.5	N/A
Arctic Alumina	Aluminum oxide	1.6	50-200
Arctic Silver 5	Silver, Aluminum oxide	4.1	50-200
IceFusion	Aluminum Oxide	1.2	N/A

Figure 2.10: Optical image of graphene nanopowder with average thickness of 12 nm.

Graphene nanopowder A-12 was obtained from Graphene Supermarket. The flakes has an average thickness of 3 nm, between 3-8 monolayers of graphene, Figure 2.10. The dry powder has a 99.2% purity and 2.25 g/cm^3 density. Ethyl alcohol is used to ease the mixing process. Figure 2.11 shows the Raman spectrum of A-12 graphene Nano-powder used. Raman spectroscopy was conducted at 488 nm and 2.8 mW laser power. The resulting spectrum signature corresponds to a multilayer graphene [10].

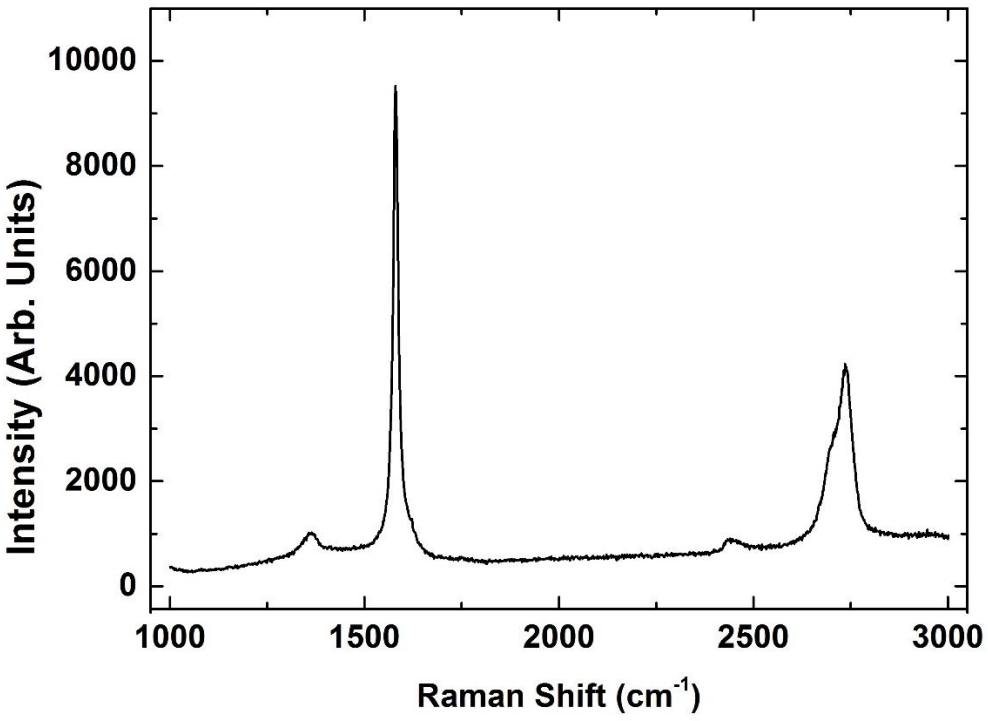

Figure 2.11: Raman spectrum of A-12 graphene powder showing a multilayer graphene spectra signatures.

2.3 Solar Cells Used

Several types of single-junction and multi-junction solar cells were tested in this dissertation. We will go through them briefly here. The first small panel used is the one seen in Figure 2.12 and it's a single-junction polycrystalline silicone solar cell. It has a manufacture rating for short circuit current of 120 mA, and an open circuit voltage of 11 V.

Figure 2.12: Single-junction polycrystalline silicon solar panel.

The second small solar panel was also a single-junction polycrystalline silicon solar cell but at a smaller size to allow us to concentrate more sunlight into it. It is seen in Figure 2.13 and it has a manufacture rating of 80 mA short-circuit current (I_{SC}) and a 3.6 Volts for an open-circuit voltage (V_{OC}).

Figure 2.13: Single-junction polycrystalline silicon solar panel.

Then we have the multi-junction solar cells seen at Figure 2.14 and Figure 2.15. They have an open-circuit voltage of 2.4 V and a short circuit current of 4 mA. They were used under a high concentration of 1000+ suns.

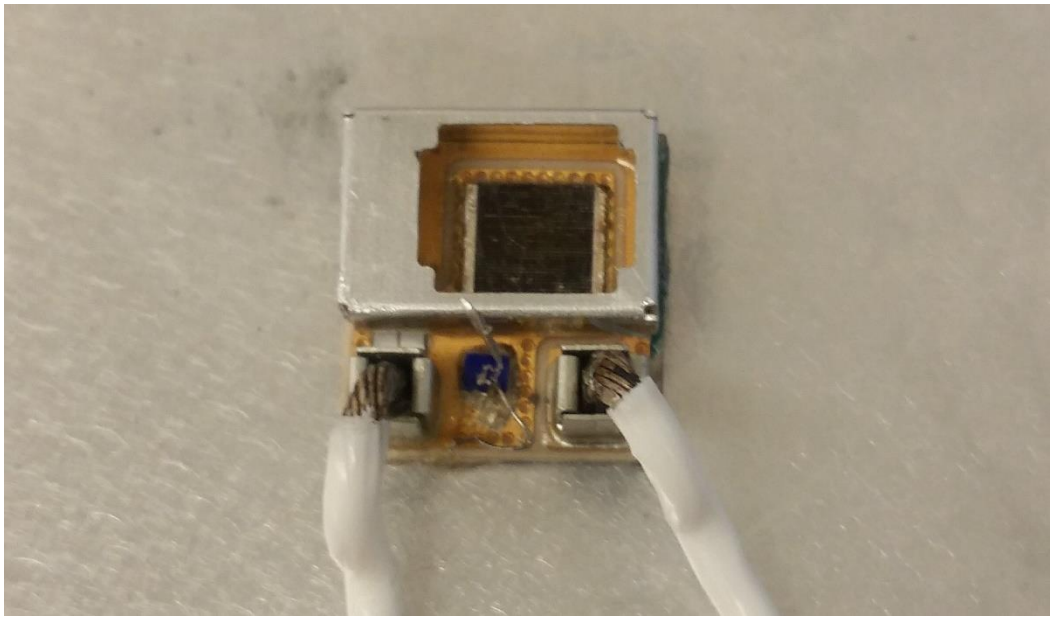

Figure 2.14: Optical image of multi-junction solar cell.

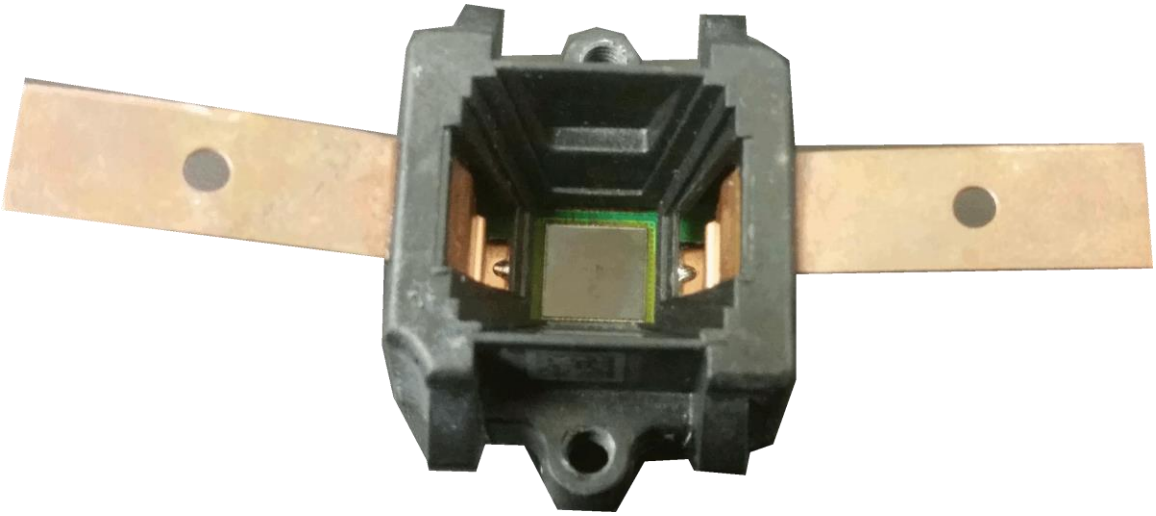

Figure 2.15: Optical image of multi-junction solar cell.

2.3 Experimental Procedure

The basic steps of the TIMs mixing and testing process is outline in Figure 2.16. The thermal interface material was weighed by the precision electronic balance and added to a beaker. The weight measurements were noted to the milligram precision. After that, a small amount of 12 nanometer graphene nanopowder was added to the paste in accordance with the following weight percentage formula:

$$Graphene\ wt\% = \frac{Graphene\ Weight}{TIM\ Weight + Graphene\ Weight} \tag{2.1}$$

The volume fraction is found by using the following equation:

$$Graphene\ Vol\% = \frac{Graphene\ Weight}{Graphene\ Density} \div \left(\frac{Graphene\ Weight}{Graphene\ Density} + \frac{TIM\ Weight}{TIM\ Density}\right)$$

Table 2.2 shows the different types and weights of thermal interface materials and phase change material used, the graphene weight and calculated weight fraction and volume fraction.

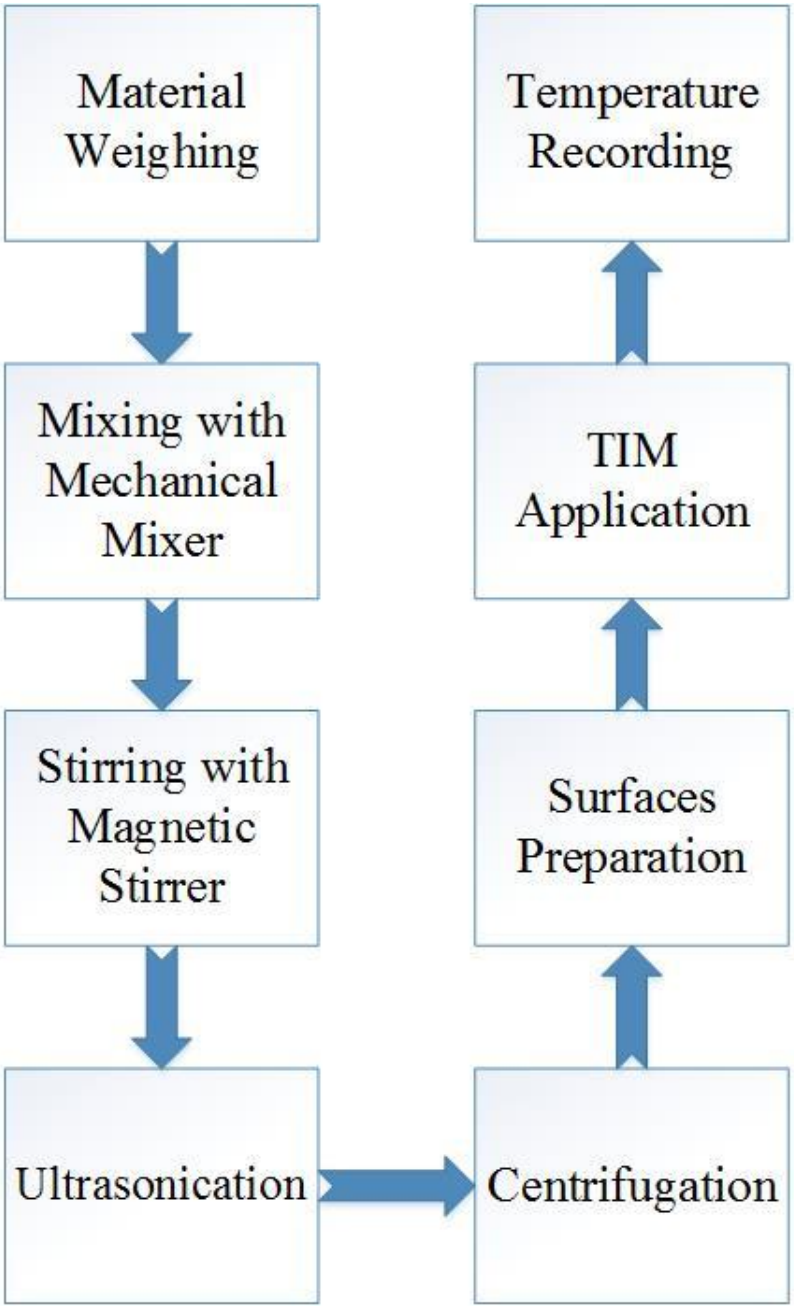

Figure 2.16: Basic steps of TIMs mixing and testing

Table 2.2: Weights of thermal interface materials and graphene that were mixed together along with graphene wt% and %vol.

TIM Type	TIM Weight (mg)	Graphene Weight (mg)	MLG Wt%	MLG Vol%
Arctic Alumina	1026.9	10.8	1.04%	0.74%
Arctic Alumina	5506	109.7	1.95%	1.4%
Arctic Alumina	5381	168.8	3.04%	2.18%
Arctic MX-4	1995.8	19.2	0.95%	1.06%
Arctic MX-4	2291.8	50.1	2.14%	2.37%
Arctic MX-4	831.2	25.9	3.02%	3.35%
Arctic Silver 5	4723	48.7	1.02%	1.84%
Arctic Silver 5	2214.5	48.2	2.13%	3.81%
Arctic Silver 5	2541.2	76.54	2.92%	5.2%

The compound is then mixed carefully with the addition of ethyl alcohol to aid in the mixing process. Using a mechanical mixer, the compound is mixed continuously for about 1 hour. After that, a magnetic stirrer is used to mix the compound for 3-4 hours or until most of the ethyl alcohol has evaporated. The compound is then allowed to rest for about 30 minutes. Before applying the mixed compound, both the surfaces of the solar cell and heat sinks were prepared and cleaned using special solutions of thermal material removing and a thermal surface purifying. This step insures no TIM residual remains on the surface and interferes with the current TIM tested.

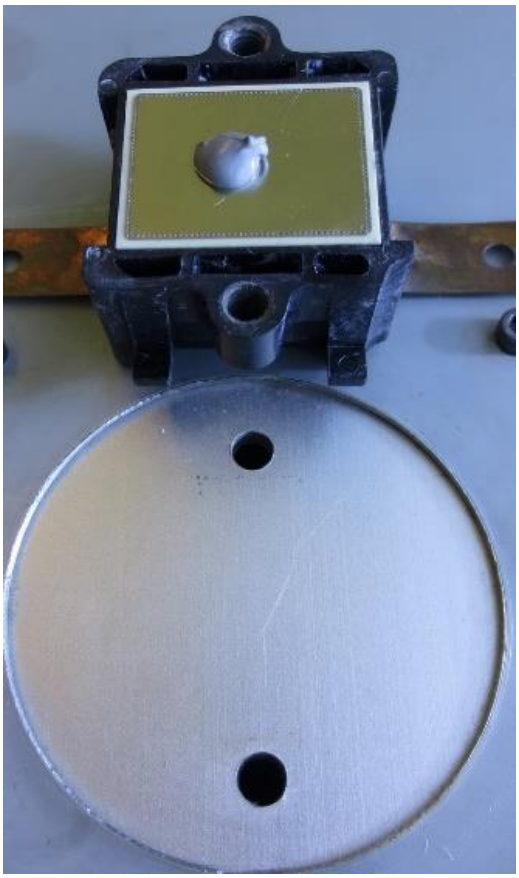

Figure 2.17: Example of application of thermal interface material.

After surfaces preparation, the mixed compound is applied in to the solar cell thermal back surface as shown in Figure 2.17. Both surfaces were then secured together by two screws. The screws were tightened to a standard torque using power screw driver. This step is to insure a uniform pressure throughout all tests. Manufacturer's recommended cure times for every TIM were observed and several thermal cycling were employed to reach optimal settings.

Using multi-channel temperature logger, the heat sinks and ambient temperatures were recorded every 10 seconds with a time and date stamp. Table 2.3 shows a sample of recorded date where two thermocouples are used to record the ambient temperature and two for the two heat sinks. The ambient temperature used for calculations is the average between the two recordings. The difference between heat sink temperature and ambient temperature (ΔT) is measured and averaged over a period of one hour. Since we're reading the temperature from the heat sink, it follows that the TIM with higher thermal conductivity would result in a higher ΔT. Similarly, the less thermal conductivity of TIM the lower ΔT will be.

Table 2.3: Sample of recorded temperature values

Date/Time	Ambient 1	Heat Sink 1	Heat Sink 2	Ambient 2
5/1/2013 18:46	22.8	41.7	43	22.4
5/1/2013 18:46	22.8	41.8	43	22.5
5/1/2013 18:46	22.7	41.9	43	22.4
5/1/2013 18:47	22.7	41.9	43	22.4
5/1/2013 18:47	22.7	41.8	42.9	22.4
5/1/2013 18:47	22.7	41.8	42.9	22.4
5/1/2013 18:47	22.5	41.3	42.4	22.3

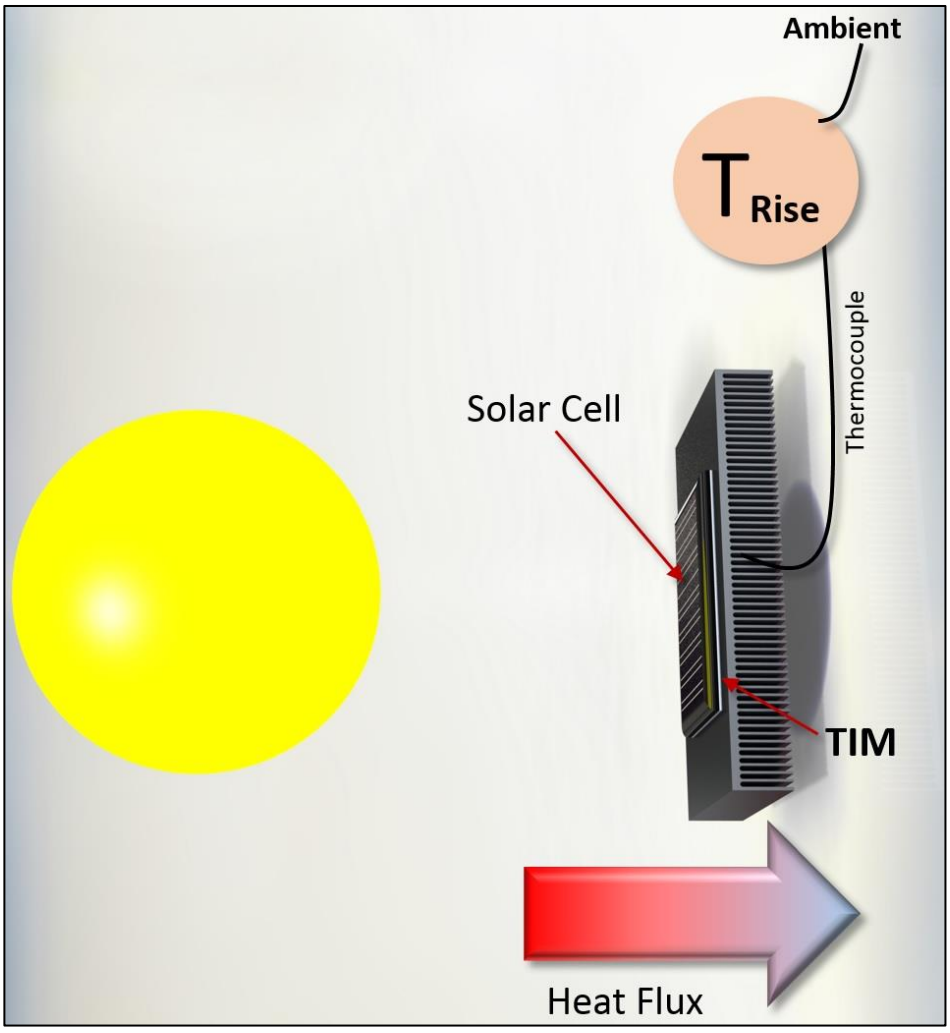

Figure 2.18: Principle of the measurements of temperature rise by taking the difference between heat sink temperature and the ambient temperature.

If a thermocouple probe is placed on the solar cell inside the enclosure, the radiation energy from the solar cell light can heat the probe and affect the reliability of the results. For this reason, we used the alternative method described above to evaluate thermal conduction as shown in Figure 2.18. Because every solar cell has its unique surface defects and exposure to light, we have used the same solar cell for all thermal interface materials

mixed. For example, all Arctic Silver Arctic Alumina mixtures were all tested on the same solar cell.

2.4 Spreading Characteristics of TIMs

Different TIM pastes have different spreading characteristics. When applying TIM and joining the two surfaces, it is important that the TIM spreads under applied pressure to cover the entire contacting area between the two surfaces. A typical spreading behavior can be seen in Figure 2.19 where the TIM has covered the entire surface. Using insufficient amount of TIM can result in spreading similar to the one shown in Figure 2.20 where the TIM has not spread to cover the entire surface and the remaining uncovered portion can cause an increase in the thermal resistance.

Figure 2.19: Typical spreading of thermal interface material.

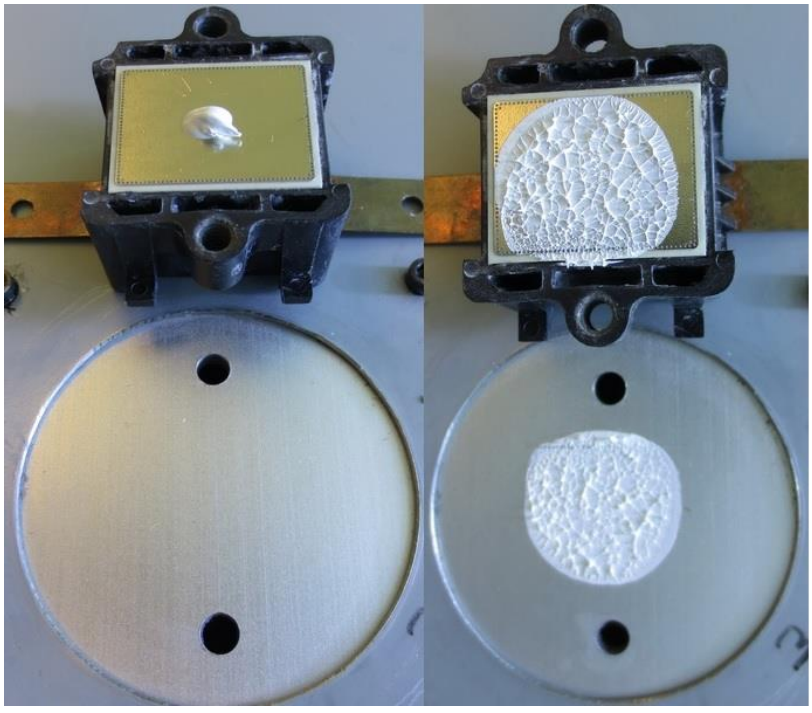

Figure 2.20: Insufficient use of TIM causing poor spreading of thermal interface material.

On the other hand, using excessive amount of TIM can increase the bond-line thickness, BLT, of the TIM and result in an increase in the overall thermal resistance Figure 2.21.

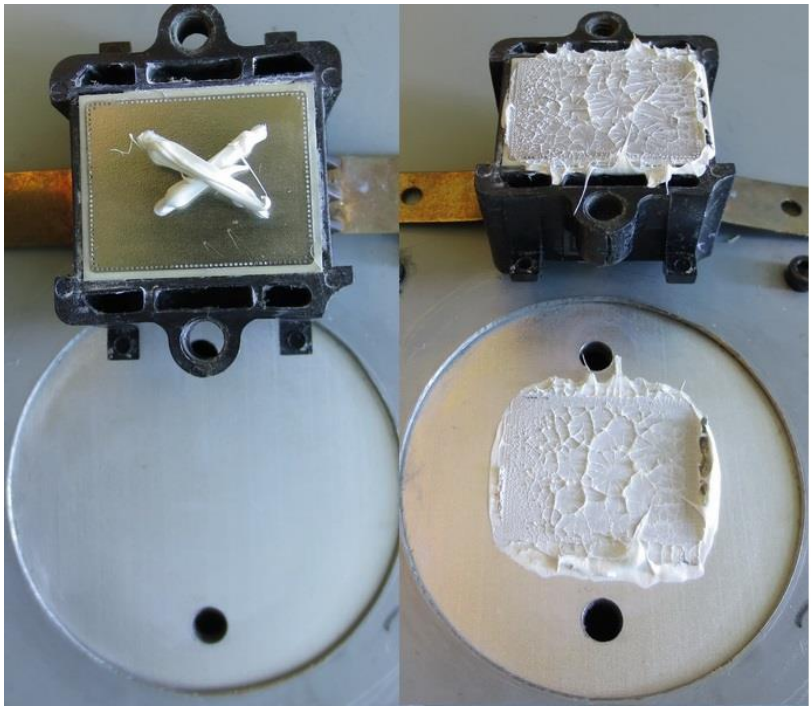

Figure 2.21: Excessive use of thermal interface material can increase the bond-line thickness BLT.

The way TIM spreads is also affected by the density and viscosity of the TIM. Figure 2.22 shows the poor spreading of a TIM due to its high density and low viscosity. In such case, a manual spreading of the TIM is required where a thin layer of the paste is evenly spread over the contact surface using a plastic spreader tool, Figure 2.23.

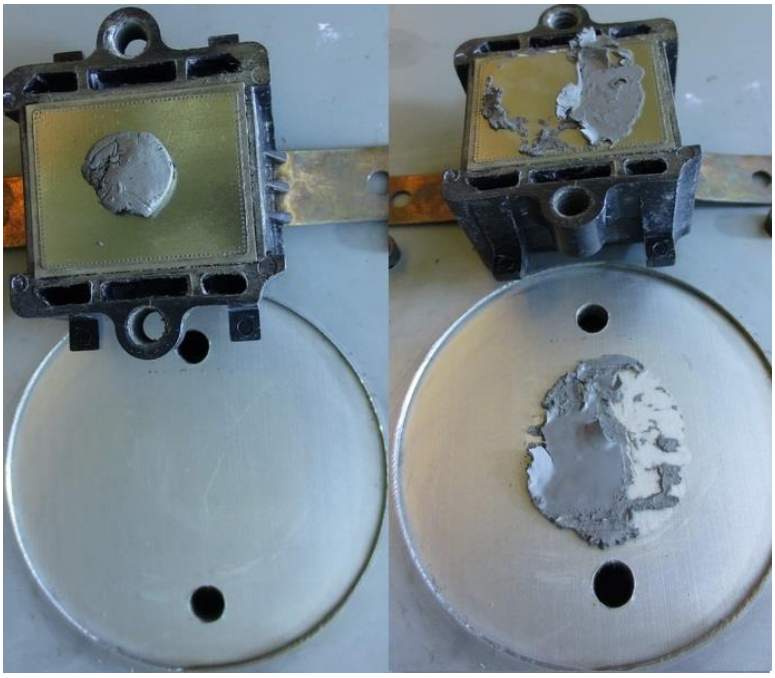

Figure 2.22: Weak spreading of thermal interface material caused by the high density and low viscosity of the compound.

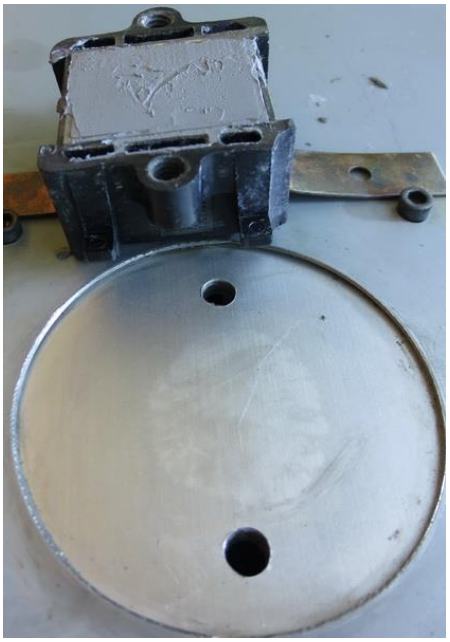

Figure 2.23: Manual spreading of thermal interface material.

2.5 Validity and Reliability of Data

Great care has been undertaken to insure the accuracy of measurements and similarity of test trials. However, there are some limitation factors that must be addressed like device's accuracy and surface's degradations. One important factor that changes with every trial is the TIM application method. No two trials have the exact same TIM spreading due to changes in the TIM viscosity with each addition of dry graphene powder. Another factor is the degradation of the solar cell and heat sink's surfaces with use over time. More scratches and surface defects are introduced to both surfaces which results in a change in the measured data. Figure 2.24 shows the surface scratches developed from continuous usage.

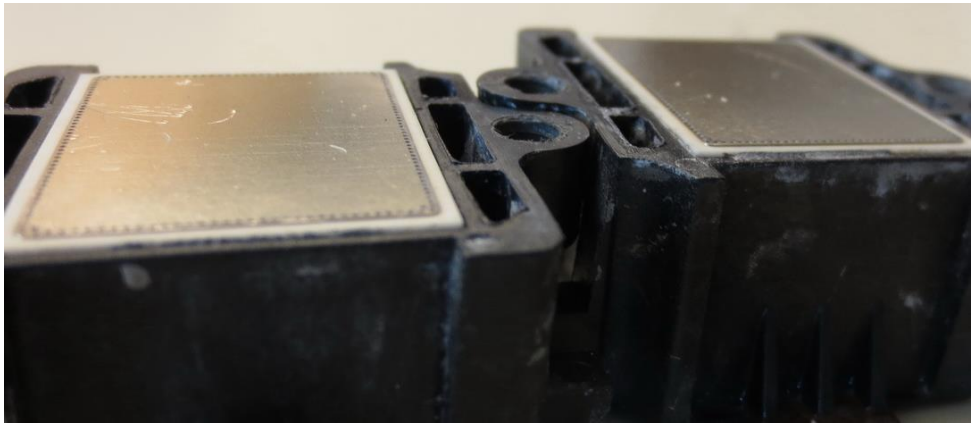

Figure 2.24: Contact surfaces can develop surface defects arising from continuous testing of the same heatsinks and back plates.

References

[1] I. A&D ENGINEERING, "HR-60 analytical balance Manual," p. 40, 2013.

[2] I. Applent Instruments, "AT4516 Multi-Channel Temperature Meter " p. 5, 2011.

[3] Oriel, Newport Coorporation, "Oriel Product Training Manual " p. 9, 2006.

[4] Analysis Tech, "Thermal Interface Material Tester Operation Manual, TIM Tester 1300/1400 " p. 1, 2013.

[5] NETZSCH-Gerätebau GmbH, "Operating Instructions, Nano-Flash-Apparatus, LFA 447" p. 1, 2009.

[6] I. Arctic Silver, "Arctic Silver 5 MSDS," p. 2, August 23, 2012 2012.

[7] I. Arctic Silver, "Arctic Alumina MSDS," p. 2, August 23, 2012 2012.

[8] A. AG, "ARCTIC MX-4 Spec Sheet," p. 2, 2013.

[9] CoolMaster, "IceFusion Spec Sheet," p. 1, 2011.

[10] Ferrari, Andrea C., J. C. Meyer, V. Scardaci, C. Casiraghi, Michele Lazzeri, Francesco Mauri, S. Piscanec et al. "Raman spectrum of graphene and graphene layers." Physical review letters 97, no. 18 (2006): 187401.

Chapter 3

Results and Inference

3.1 Results: Solar Module

Several commercial TIMs loaded with 1-3 wt% graphene were tested between interfaces of solar cell and heat sink. Their thermal conductance was evaluated as a function of ΔT, the difference between heat sink and ambient temperatures. Temperature values were taken after observing recommended TIM cure times and thermal cycling. TIMs with higher thermal conductivity transfer more heat from the solar cell to the heat sink, which then leads to an increase in the heat sink temperature. The change in ambient temperature over time and between test trials causes a change in the internal temperature of the testing module. Therefore, the ambient temperature is subtracted from the heat sink temperature to account for this change.

3.1.1 Arctic MX-4

Figure 3.1 compares ΔT for Arctic MX-4 at different graphene wt% loading (0%-3%) over time. The 0% line represents the reference value of the TIM with no graphene being added to it.

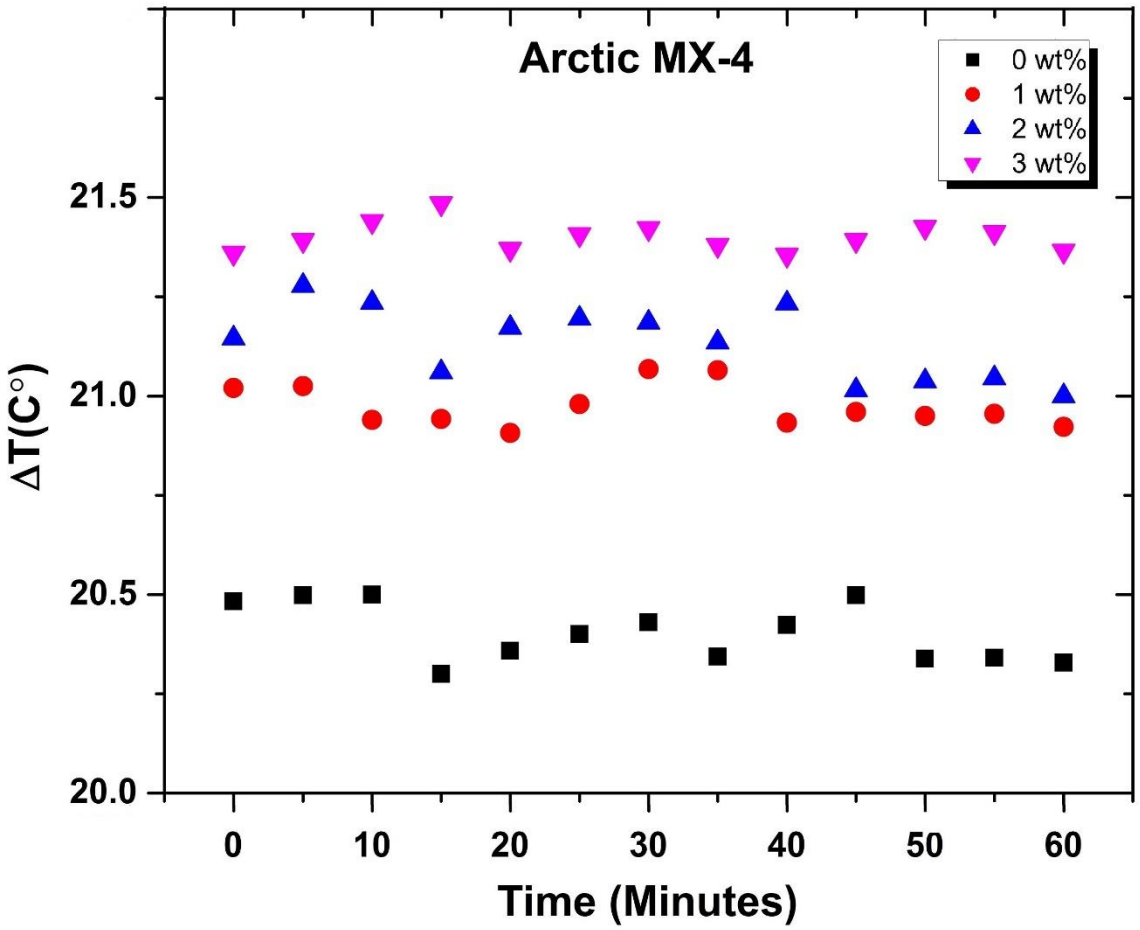

Figure 3.1: Temperature rise over time for Arctic MX-4 mixed with 0-3 wt% graphene.

For the sake of comparison, and despite the Arctic MX-4 manufacturer indication of no cure time is requirement, the results were taken after curing time that matches that of the other two TIMs. By averaging the individual ΔT measurement for each of the four compounds tests (0-3 wt%) over an hour, we can see that ΔT increase with increasing graphene weight fraction as shown in table 3.1.

Table 3.1: average and percentage increase of ΔT for Arctic MX-4 with (0-3) graphene wt%.

Graphene wt%	Average ΔT (°C)	ΔT Increase (%)
0%	20.38	0%
1%	20.92	2.65%
2%	21.1	3.53%
3%	21.4	5.01%

The increase of ΔT as a function of graphene weight fraction for Arctic MX-4 is illustrated in Figure 3.2. The increase in ΔT as a result of using more graphene weight fraction is evident. From this we conclude that the performance of Arctic MX-4 TIM is enhanced when adding graphene powder as filler.

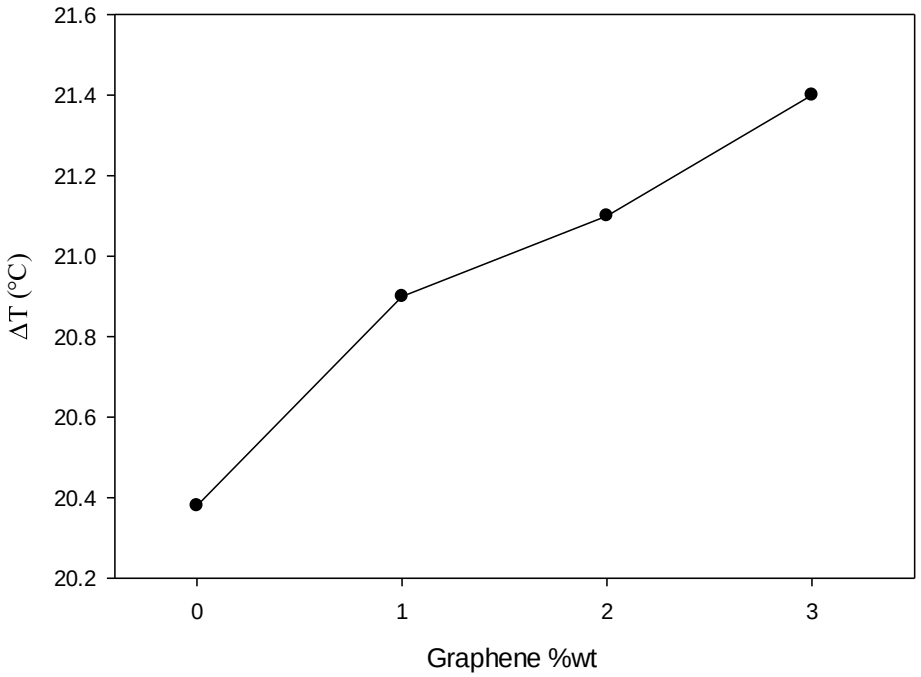

Figure 3.2: : Temperature rise as a function of graphene weight fraction for Arctic MX-4.

3.1.2 Arctic Alumina

Figure 3.3 illustrates ΔT as a function of time resulting from the four Arctic Alumina compounds tested at graphene weight fraction from 0%-3%. The performance of this TIM improved more significantly when using graphene as a filler, with 12.1% increase in ΔT when using 3% graphene weight fraction compared to no graphene usage. The averaged ΔT for the four trials of Arctic Alumina are listed in table 3.2.

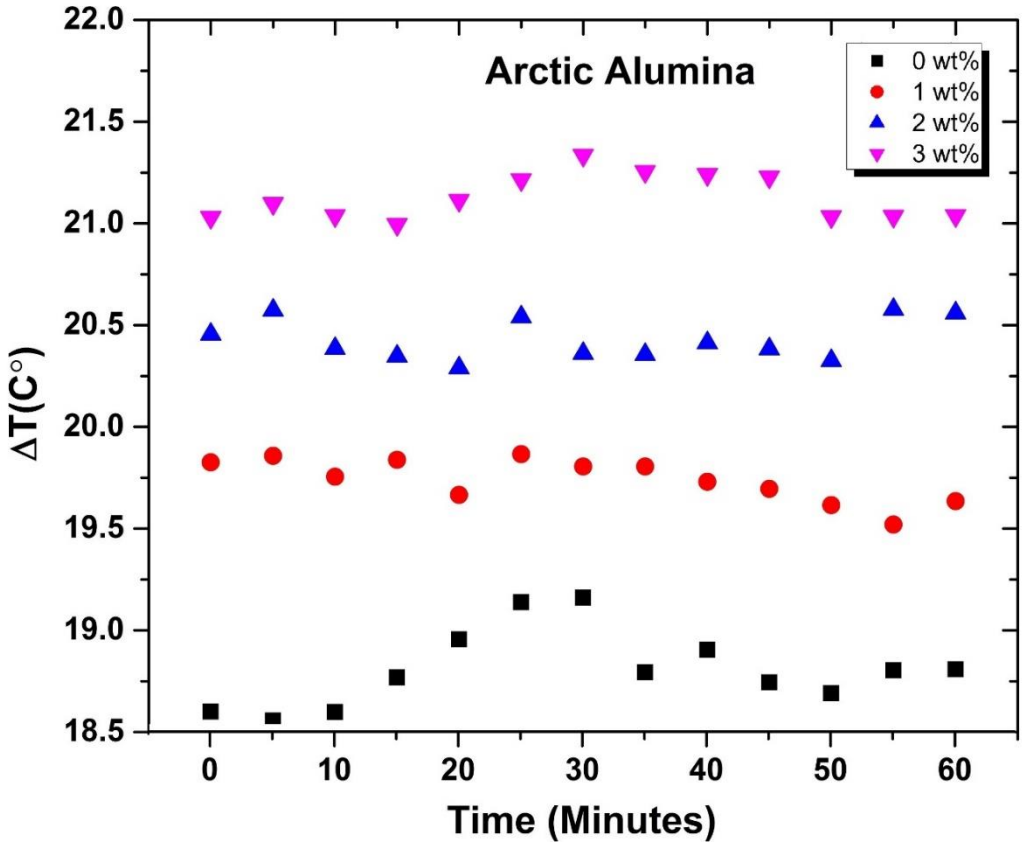

Figure 3.3: Temperature rise over time-for Arctic Alumina mixed with 0-3 wt% graphene.

Table 3.2: Average and percentage increase of temperature rise for Arctic Alumina with (0-3) graphene wt%.

Graphene wt%	Average ΔT (°C)	ΔT Increase Percentage
0%	18.79	0%
1%	19.69	4.8%
2%	20.38	8.5%
3%	21.07	12.1%

Figure 3.4 shows ΔT as a function of graphene weight fraction for Arctic Alumina. A steady and more visible increase in ΔT with each additional graphene weight fraction can be seen.

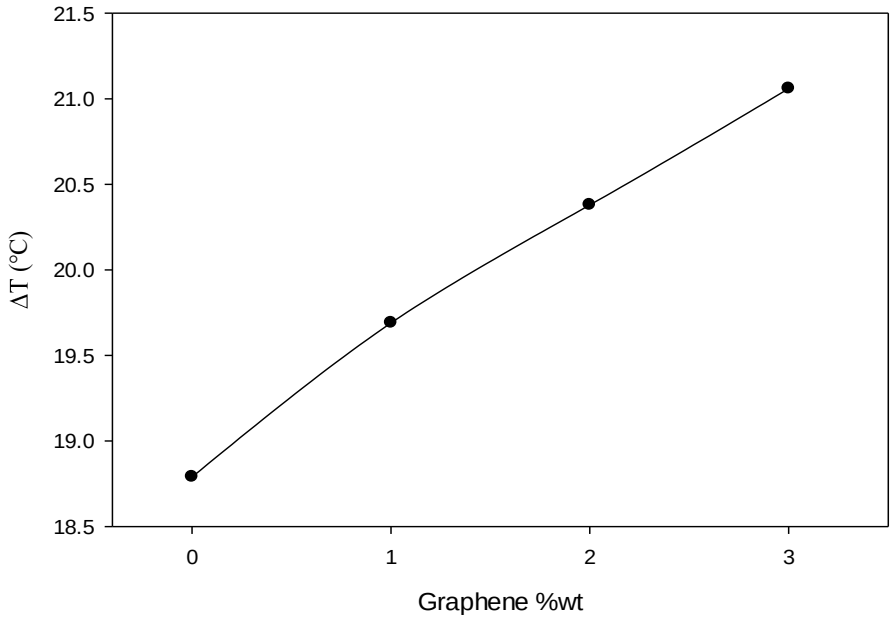

Figure 3.4: Temperature rise as a function of graphene weight fraction for Arctic Alumina.

3.1.3 Arctic Silver 5

The measured ΔT for the four Arctic Silver 5 compounds can be seen in Figure 3.5. This TIM exhibits less performance change with each increase in graphene wt%. Only an increase of 2.44% in ΔT is resulted from adding 3% weight fraction of graphene. Table 3.3 shows the average and percent increase of ΔT for the four trials of Arctic Silver 5.

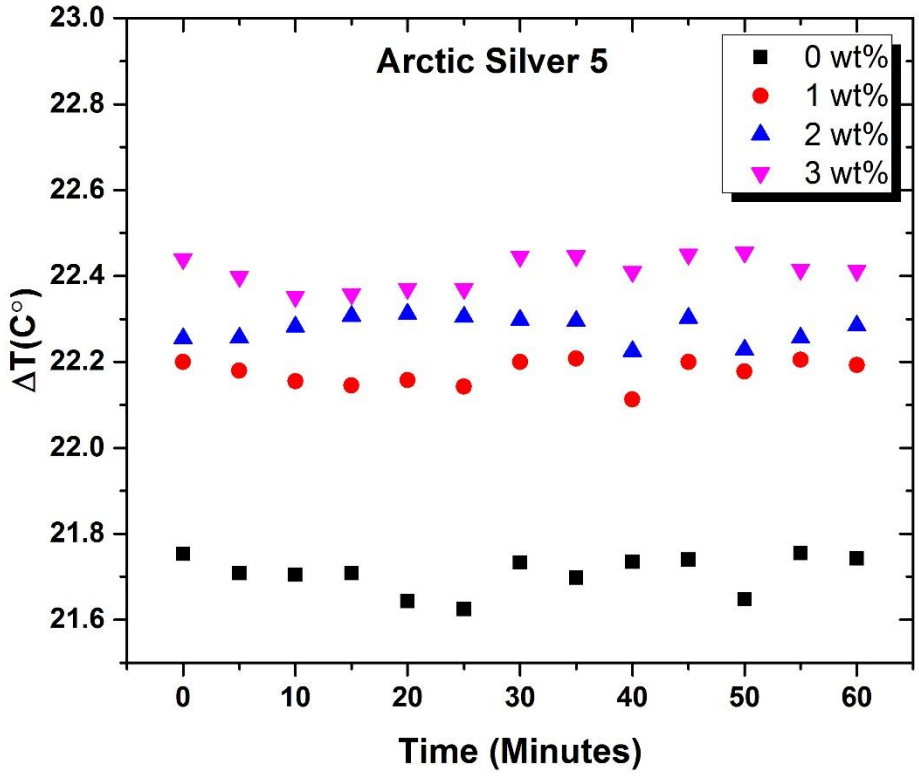

Figure 3.5: Temperature rise over time-for Arctic Silver 5 mixed with 0-3 wt% graphene.

Table 3.3: average and percentage increase of ΔT for Arctic Silver 5 with (0-3) graphene wt%.

Graphene wt%	Average ΔT (°C)	ΔT Increase Percentage
0%	21.72	0%
1%	22.18	2.12%
2%	22.23	2.35%
3%	22.25	2.44%

Figure 3.6 shows temperature rise increasing as a function of graphene weight fraction used.

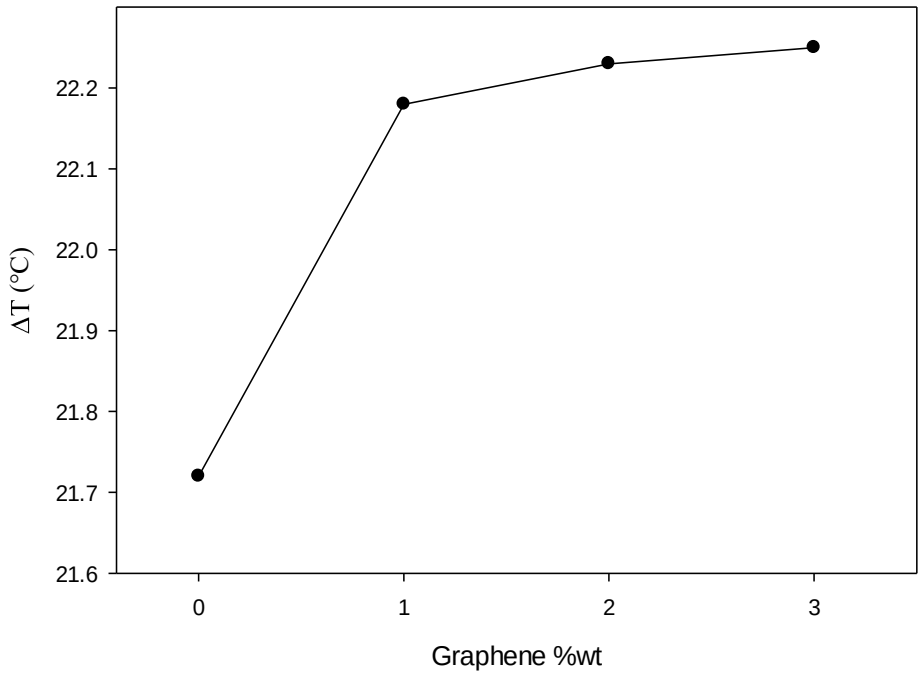

Figure 3.6: Temperature rise as a function of graphene weight fraction for Arctic Silver 5.

3.2 Solar Simulator

Several measurements were done under the solar simulator. The two subsections below will describe results obtained from testing under the Oriel Solar Simulator under non-concentrated and concentrated light intensities.

3.2.1 Non-Concentrated Solar Light

Many research has been done on solar cells and effects of temperature on photovoltaics [1-11]. To illustrate the effects of temperature on solar cells, a single-junction polycrystalline silicon small solar panel is placed under the solar simulator with no cooling whatsoever. As seen in Figure 3.7, initially we start by switching the solar simulator on and the solar panel is subjected to sunlight, the open-circuit voltage starts to drop as the temperature of the solar panel is rising. After 10 minutes of operation and 30° C increase in the panel temperature, we see that the open circuit voltage has dropped about 12%. The following 10 minutes, as seen in the Figure, the solar simulator was shut off and the solar cell starts to cool off. The open-circuit voltage dropped immediately to 3.2 volts, which is due to ambient light in the laboratory. As the panel cools off, the voltage starts to rise gradually demonstrating the effects of temperature on open-circuit voltage. This cycle is repeated several times as seen in the Figure with same outcome each time.

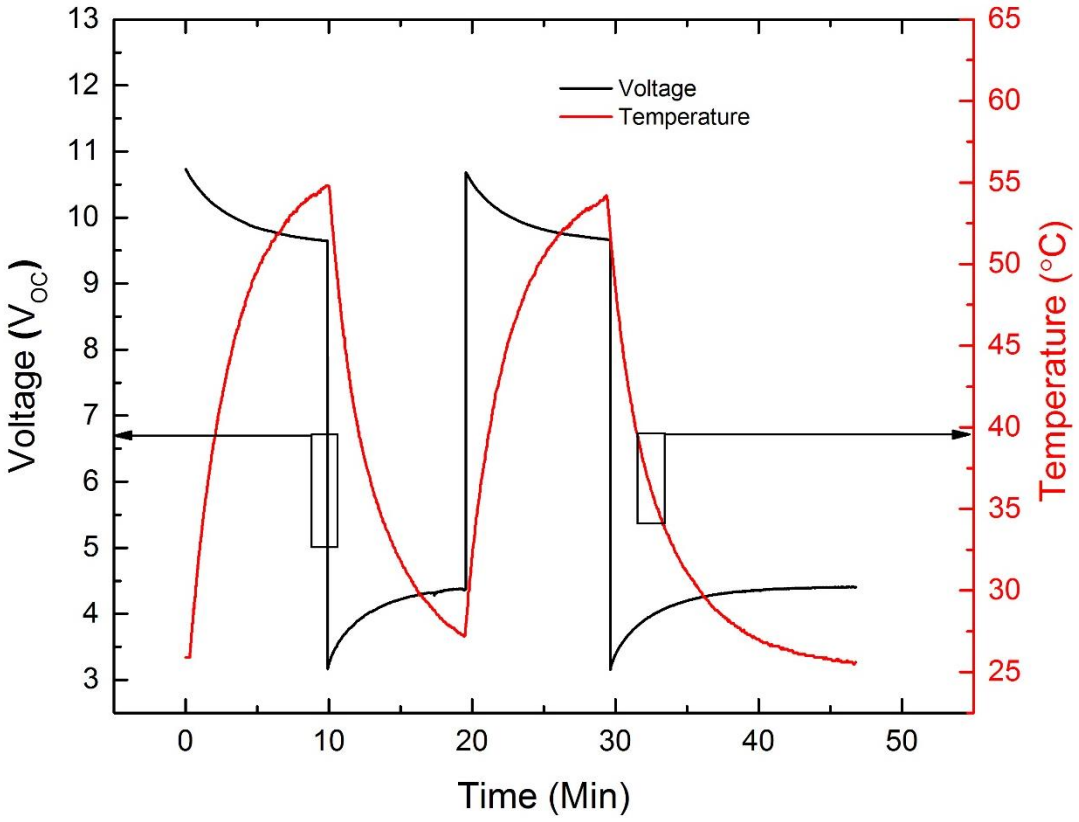

Figure 3.7: Temperature effects on the open circuit voltage (V_{OC}). Reprinted with permission from Saadah, Mohammed, Edward Hernandez, and Alexander A. Balandin. "Thermal Management of Concentrated Multi-Junction Solar Cells with Graphene-Enhanced Thermal Interface Materials." Applied Sciences 7, no. 6 (2017): 589.

To limit the impact on solar cell output, we add a heat sink to dissipate some of the solar panel temperature. As seen in Figure 3.8, which demonstrate the open-circuit voltage output under various cooling and non-cooling tests, and just by adding a heat sink we have saved almost half of the power lost due to temperature rise. When adding a thermal interface material between the heat sink and the solar panel, we see that the drop in open-circuit voltage is even less. Additionally, we have conducted the same test thermal interface

material mixed with 2-6 wt% graphene, and as seen in the graph, a 6 wt% of graphene has saved more than 75% of the power lost due to panel heat. Table 3.4 demonstrate the numerical values of each test result [12].

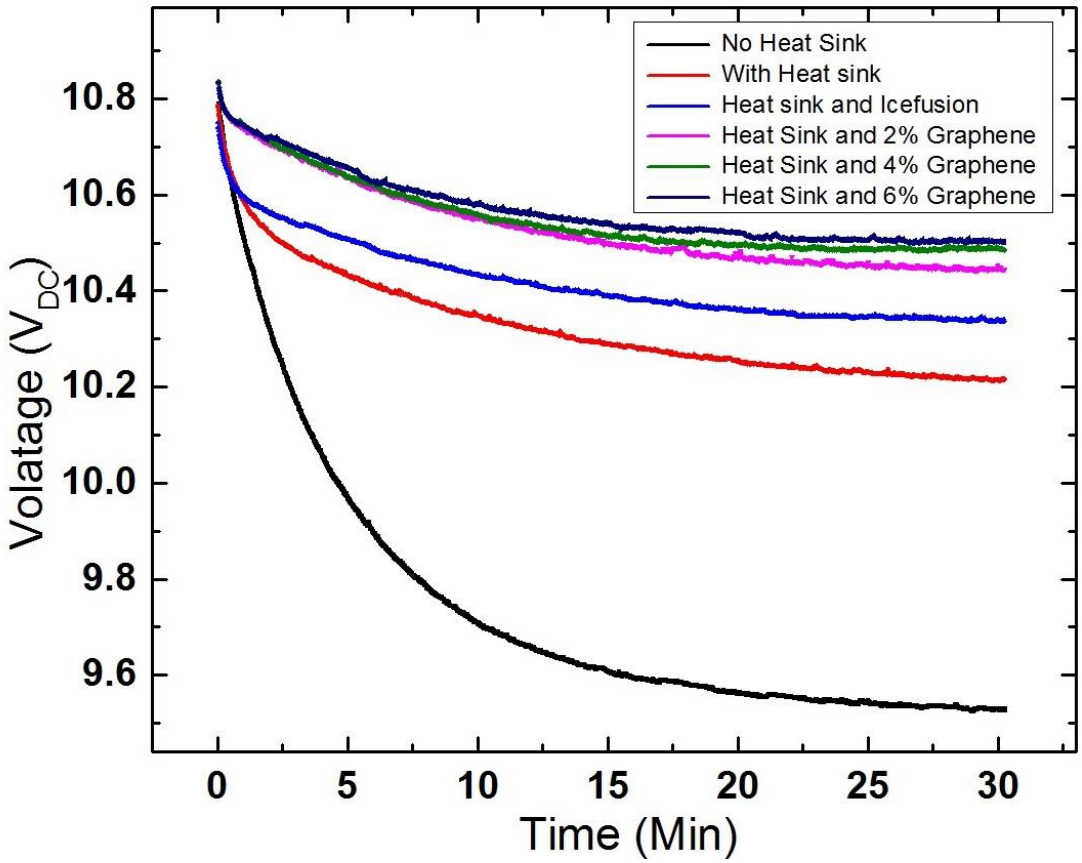

Figure 3.8: Open circuit voltage (V_{OC}) measured with and without cooling at 1 sun concentration Reprinted with permission from Saadah, M., D. Gamalath, E. Hernandez, and A. A. Balandin. "Graphene-enhanced thermal interface materials for heat removal from photovoltaic solar cells." In SPIE Nanoscience+ Engineering, pp. 99320H-99320H. International Society for Optics and Photonics, 2016.

Table 3.4: Open-circuit voltage of the solar panel tested under 1 sun concentration and with various cooling methods.

Cooling method	**Open-Circuit Voltage**	**Percentage of V_{OC} drop**
No cooling	9.52	11.9%
Heat sink only	10.2	5.5%
TIM with 0% Graphene	10.33	4.35%
TIM with 2% Graphene	10.43	3.43%
TIM with 4% Graphene	10.49	2.87%
TIM with 6% Graphene	10.51	2.68%

It is worth mentioning that the temperature had little effect on the solar panel output short circuit current. As seen in Figure 3.9, the short-circuit current has risen less than 0.5% when the panel temperature had gone 30° C higher.

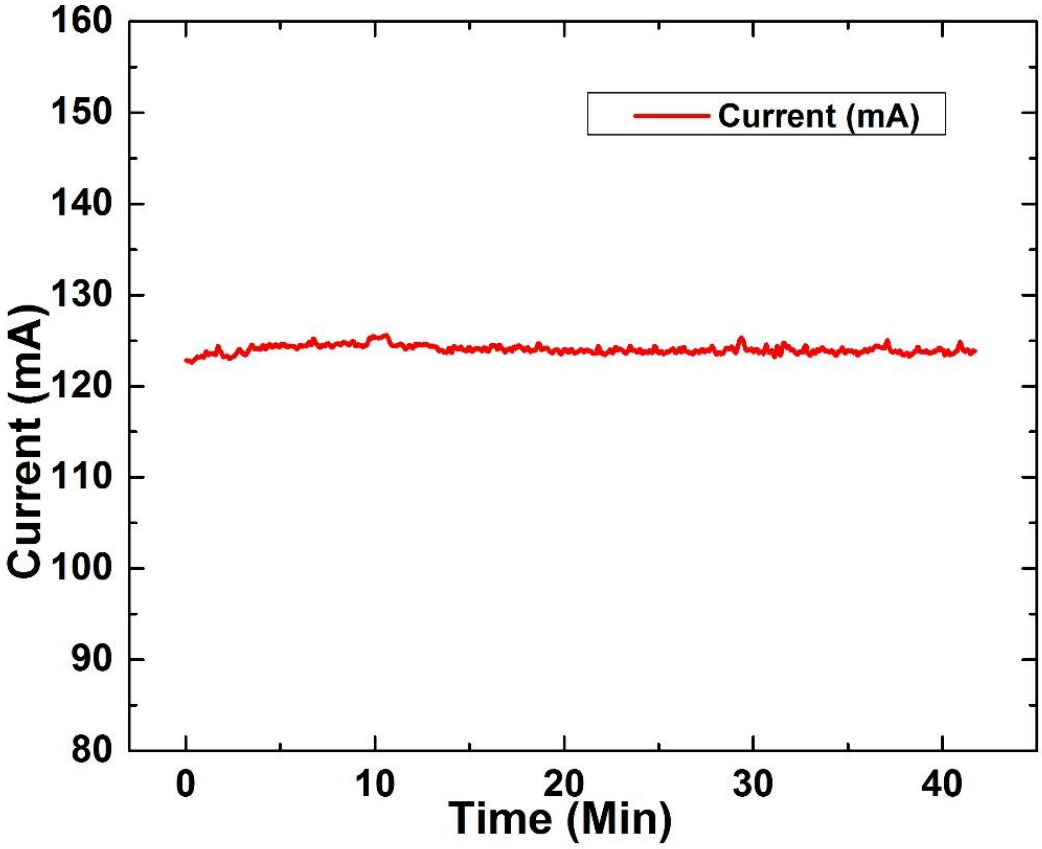

Figure 3.9: Temperature has little effect on short circuit current.

3.2.2 Concentrated Solar Light

Thus far, we have tested our solar cells under 1 sun concentration. With many research going on concentrated photovoltaics [13-21], we have sought to test different kinds of solar cells under concentrated solar light and see the effects of the significant rise in their temperature and how we can eliminate some of it. In order to do that, we have inserted a convex optical lens inside the solar simulator between its output and the solar cell. It is worth noting that with we cannot go to high concentrations when using polycrystalline silicone solar cells since they cannot withstand high temperatures. Figure

3.10 shows the temperature rise of a small single-junction silicone solar panel when subjected to 1 and 3 sun concentration. From the figure we can see that a 3 sun concentration has raised the panel temperature to almost 90° C, a 65° C increase from its initial temperature compared to only 30° C increase when using 1 sun concentration.

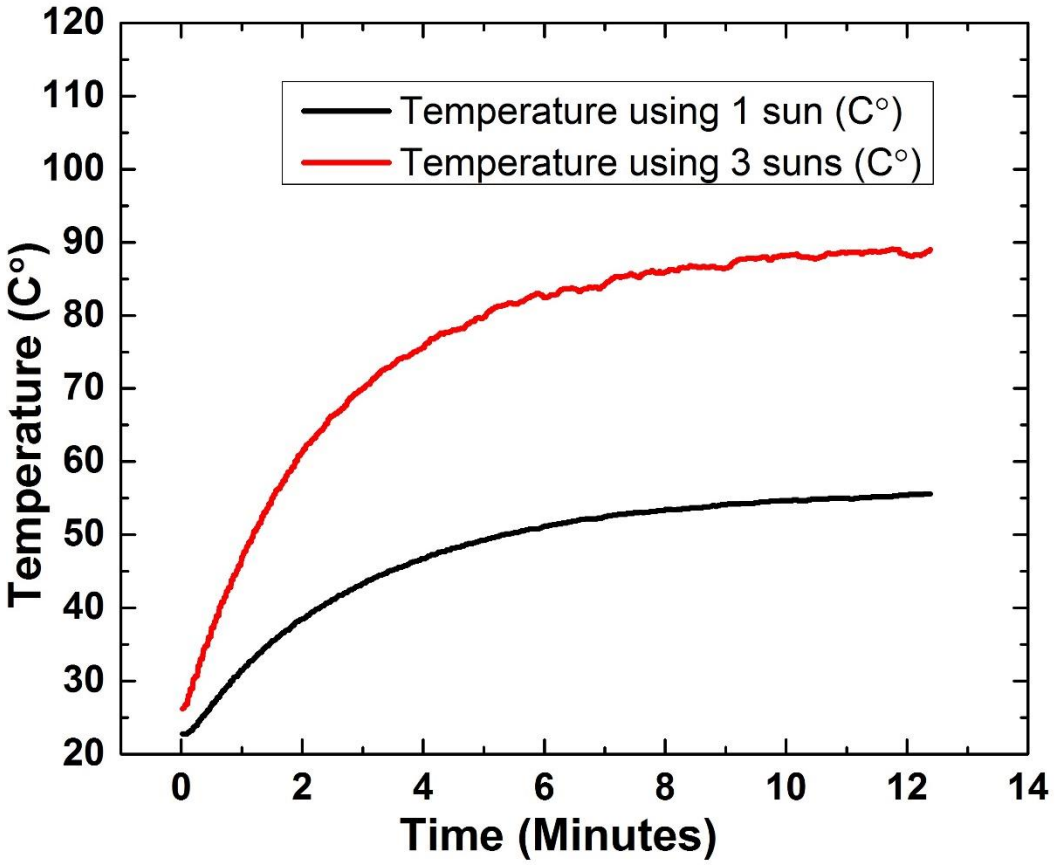

Figure 3.10: Solar cell temperature change using 1 and 3 suns concentration. Reprinted with permission from Saadah, M., D. Gamalath, E. Hernandez, and A. A. Balandin. "Graphene-enhanced thermal interface materials for heat removal from photovoltaic solar cells." In SPIE Nanoscience+ Engineering, pp. 99320H-99320H. International Society for Optics and Photonics, 2016

The significant rise in solar panel temperature when using 3 sun concentration has a more drastic effect on the solar panel open-circuit output voltage. As seen in Figure 3.11, the

initial open-circuit output voltage has risen slightly from 3.65 V when using 1 sun to 3.8 V when a 3 sun concentration is used. The output voltage then is dropped significantly by about 21% compared to 12% when using 3 and 1 suns respectively.

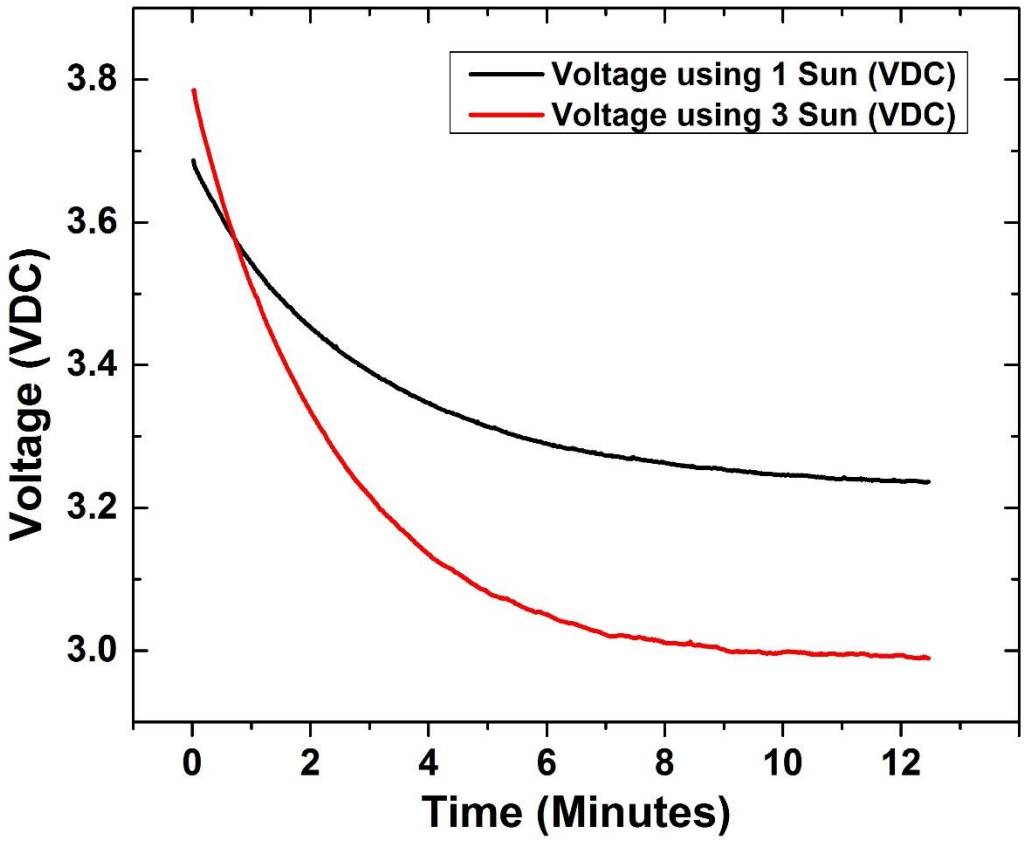

Figure 3.11: Open circuit voltage (V_{OC}) change using 1 and 3 suns. Reprinted with permission from Saadah, M., D. Gamalath, E. Hernandez, and A. A. Balandin. "Graphene-enhanced thermal interface materials for heat removal from photovoltaic solar cells." In SPIE Nanoscience+ Engineering, pp. 99320H-99320H. International Society for Optics and Photonics, 2016

In contrast to small increase in open circuit voltage due to higher concentration of sunlight, the short circuit current have increased more significantly when sunlight concentration is tripled, as seen in Figure 3.12. The 3 sun concentration have raised the

solar panel's output current from 80 mA to about 185 mA. It can also be observed that the current output has risen slightly due to the increase in solar panel temperature.

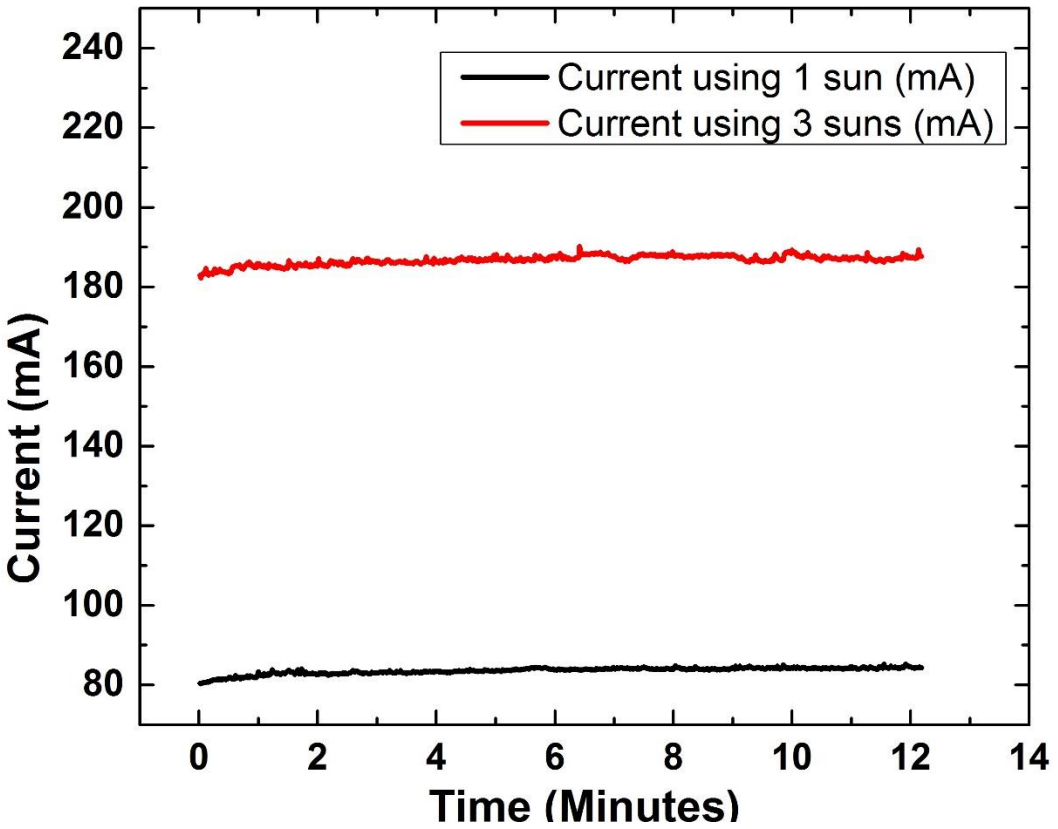

Figure 3.12: Short circuit current (I_{SC}) measured under 1 and 3 sun concentration. Reprinted with permission from Saadah, M., D. Gamalath, E. Hernandez, and A. A. Balandin. "Graphene-enhanced thermal interface materials for heat removal from photovoltaic solar cells." In SPIE Nanoscience+ Engineering, pp. 99320H-99320H. International Society for Optics and Photonics, 2016

In Figure 3.13 and Figure 3.14 we can see the effect of solar panel's temperature increase on its overall power output. The output has dropped by about 8% when using 1 sun concentration compared to a drop of 18% when 3 sun concentration is used.

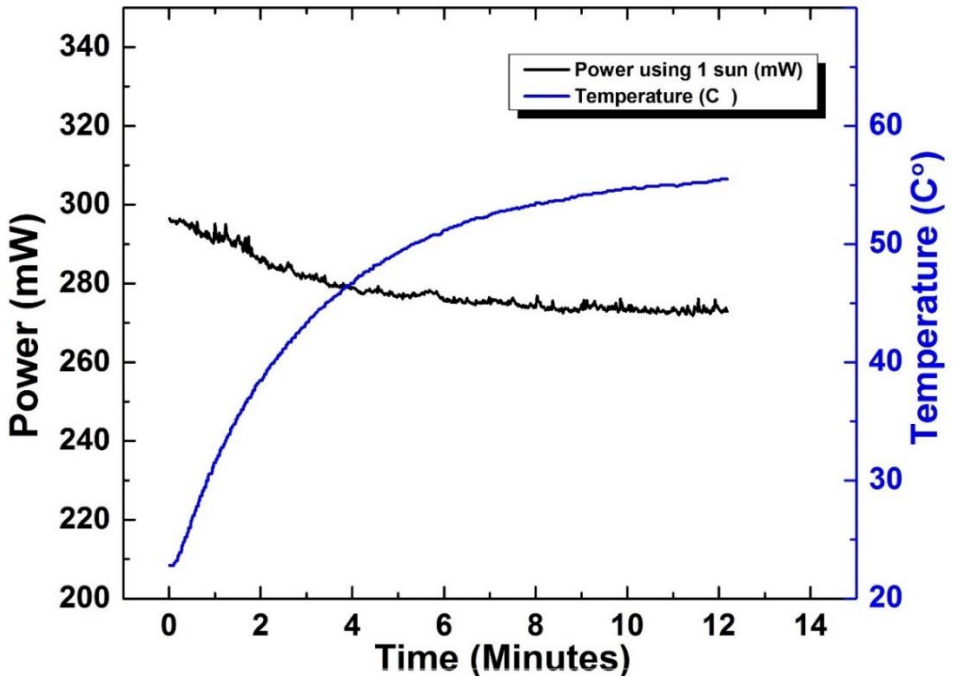

Figure 3.13: Solar cell power change with temperature increase for 1 sun concentration.

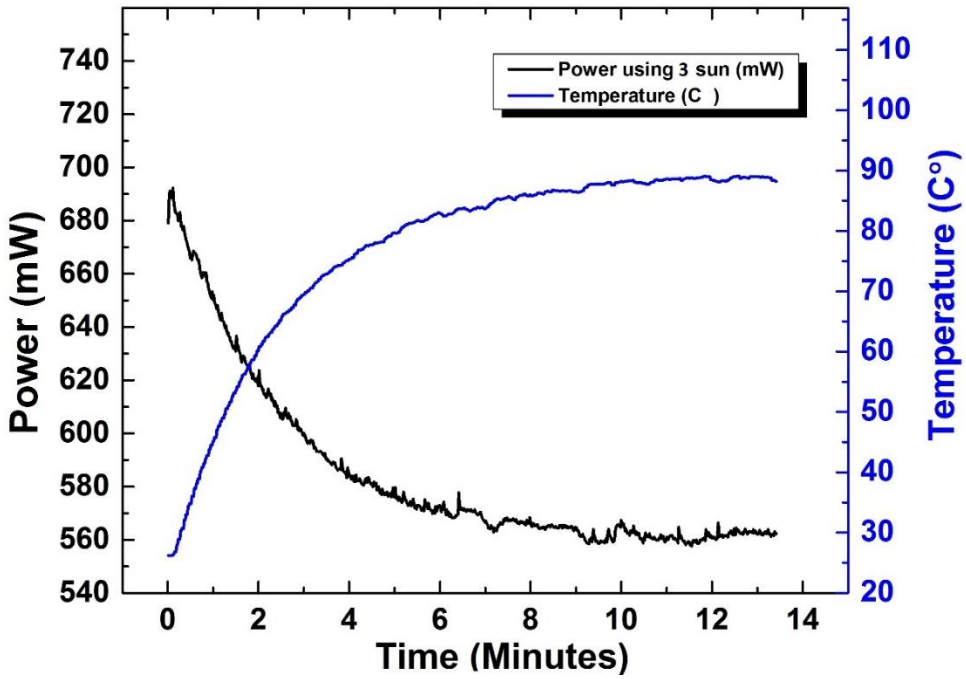

Figure 3.14: Solar cell power change with temperature increase for 3 suns concentration.

Having demonstrated the concentrated sunlight effects on single-junction silicon solar panel, we move into testing a multi-junction solar cell under concentrated sunlight

and study the effect of its temperature rise on its performance. Figure 3.15 illustrate the temperature increase of a multi-junction solar cell when subjected to 1, 6 , and 10 sun concentrations. It can be seen that it took 10 suns concentration to rise the multi-junction solar cell to 90° C, which proves that multi-junction solar cells can withstand higher concentration since it took only 3 suns to raise the temperature of a single-junction solar panel by the same amount. This is mainly because multi-junction solar cells have the ability to absorb more photon wavelengths than single-junction solar cells do.

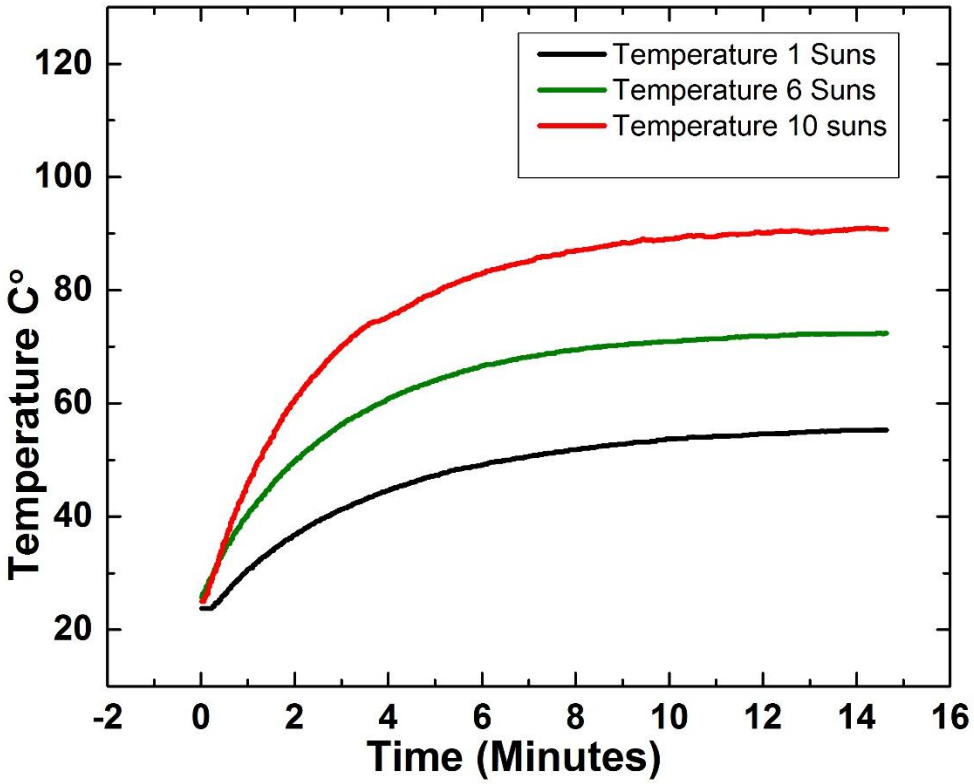

Figure 3.15: Solar cell temperature change under 1, 6, and 10, suns concentration. Reprinted with permission from Saadah, M., D. Gamalath, E. Hernandez, and A. A. Balandin. "Graphene-enhanced thermal interface materials for heat removal from photovoltaic solar cells." In SPIE Nanoscience+ Engineering, pp. 99320H-99320H. International Society for Optics and Photonics, 2016

The performance of the multi-junction solar cell has been less affected by the increase of sun concentration than single-junction solar cells. Figure 3.16 shows the drop in open circuit voltage of the multi-junction solar cell when subjected to 1, 6, and 10 suns concentration. It can be seen that the voltage output has dropped by about 16.5% when a 10 suns concentration is used, a much less drop than the 22% voltage output drop of the single-junction solar cell under only 3 sun concentration.

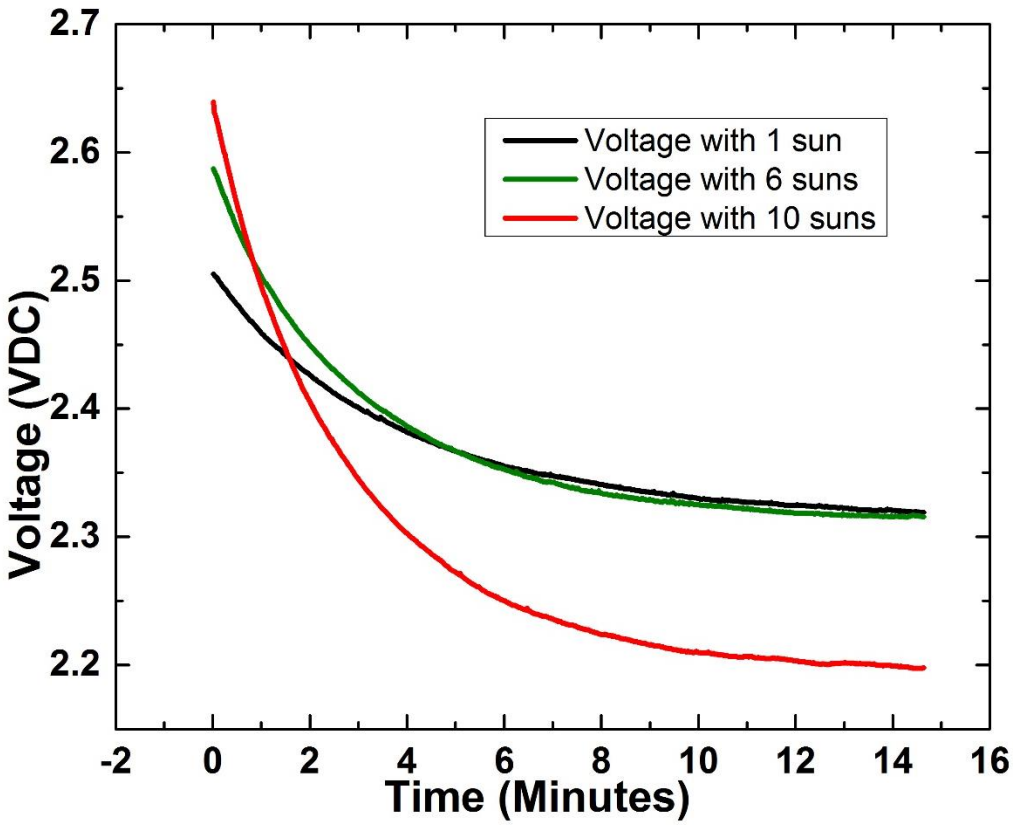

Figure 3.16: Open circuit voltage (V_{OC}) change under 1, 6, and 10 suns concentration. Reprinted with permission from Saadah, M., D. Gamalath, E. Hernandez, and A. A. Balandin. "Graphene-enhanced thermal interface materials for heat removal from photovoltaic solar cells." In SPIE Nanoscience+ Engineering, pp. 99320H-99320H. International Society for Optics and Photonics, 2016

To achieve a higher sunlight concentration, we have introduced additional lens as seen in Figure 3.17. Combined with our first large optical lens, we were able to achieve sunlight concentrations of up to 2000 suns.

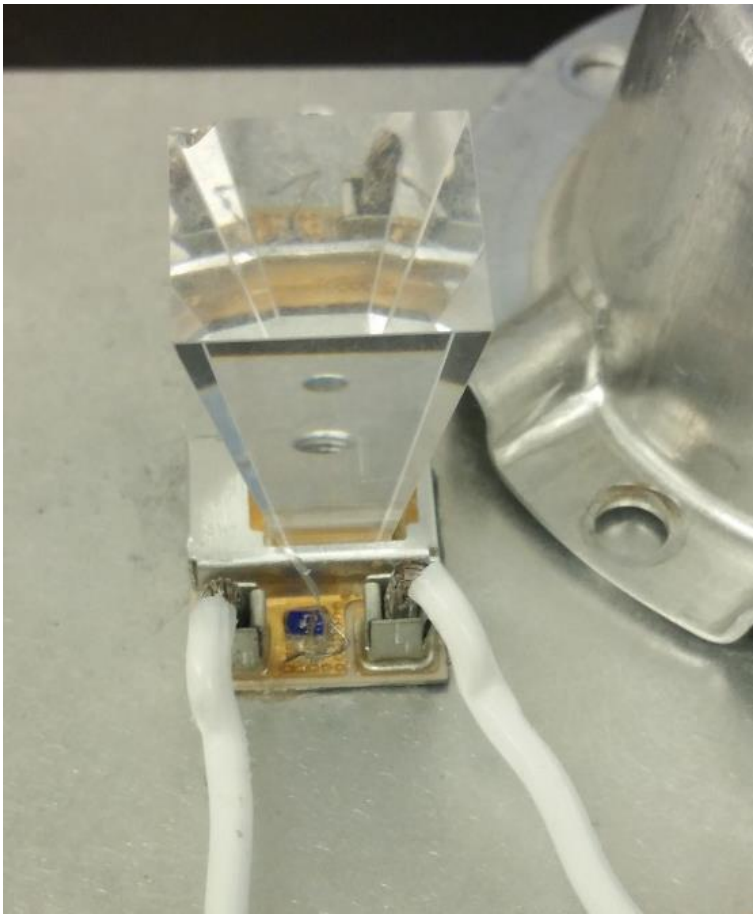

Figure 3.17: Multi-Junction solar cell with additional optical lens to achieve higher concentrations.

The V_{OC} of the multi-junction solar cell was found to increase when we increase illumination. Under 500 suns V_{OC} was 2.75 V, then 3.15 V, and 3.65 V under 1000, 1500, and 2000 sun respectively. The drop in voltage was 29% - 34% when subjected to concentrated illuminations of 500 – 2000 sun as shown in Figure 3.18 [22].

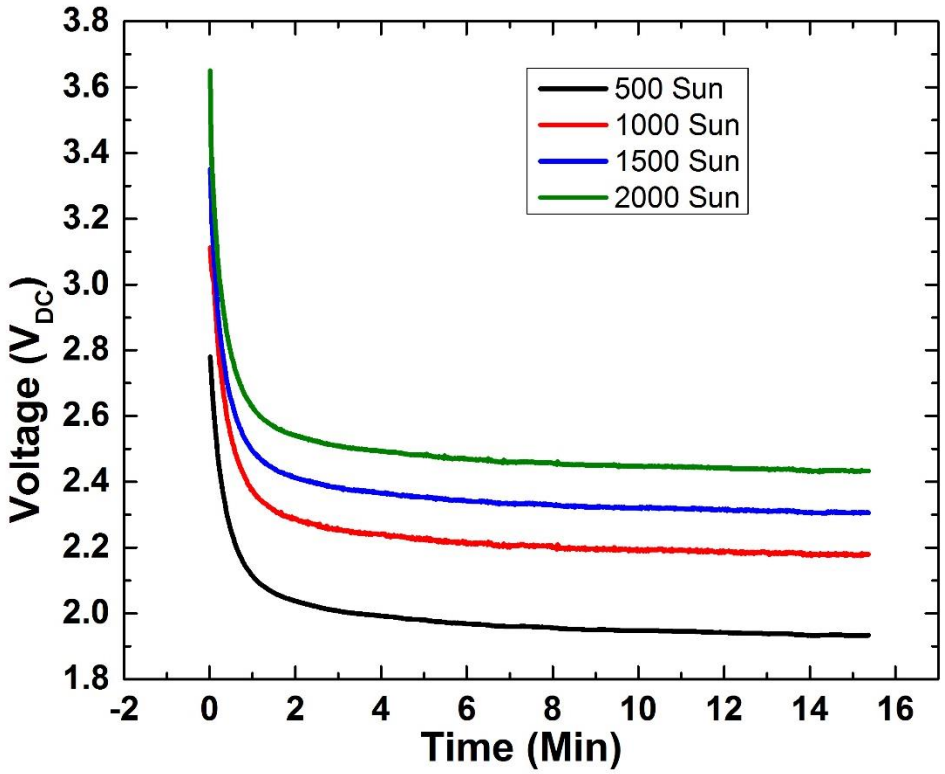

Figure 3.18: Open circuit voltage (V_{OC}) change under 500, 1000, and 2000 suns concentration. Reprinted with permission from Saadah, Mohammed, Edward Hernandez, and Alexander A. Balandin. "Thermal Management of Concentrated Multi-Junction Solar Cells with Graphene-Enhanced Thermal Interface Materials." Applied Sciences 7, no. 6 (2017): 589.

With the increased concentration, the short circuit current was found to increase linearly. However, the temperature increase of the solar cell had little effect on its output current. The measured short-circuit current was found to increase only less than 1% as the solar cell temperature increase, Figure 3.19. The overall output power of the solar cell was found to decrease due to the sharp drop of the open circuit voltage. To recover the power loss, the solar cell is attached to an aluminum heatsink and the experiment is repeated. Figure 3.20 shows V_{OC} of the solar cell under 1000 sun concentration with and without

cooling. The drop in voltage is reduced less than 12% when 4 wt% graphene TIM is used compared to 29% drop when no cooling is employed. This

thermal management technique allowed us to recover 60% of the loss in power. Figure 3.21 shows the solar cell voltage under 2000 and we can see that the voltage drop went from 0.9 V in case of 1000 suns to 1.2 V for 2000 sun concentration. The drop in the solar cell voltage was reduced from 34% to about 12%, therefore saving about 65% of the energy wasted due to the cell's heat rise.

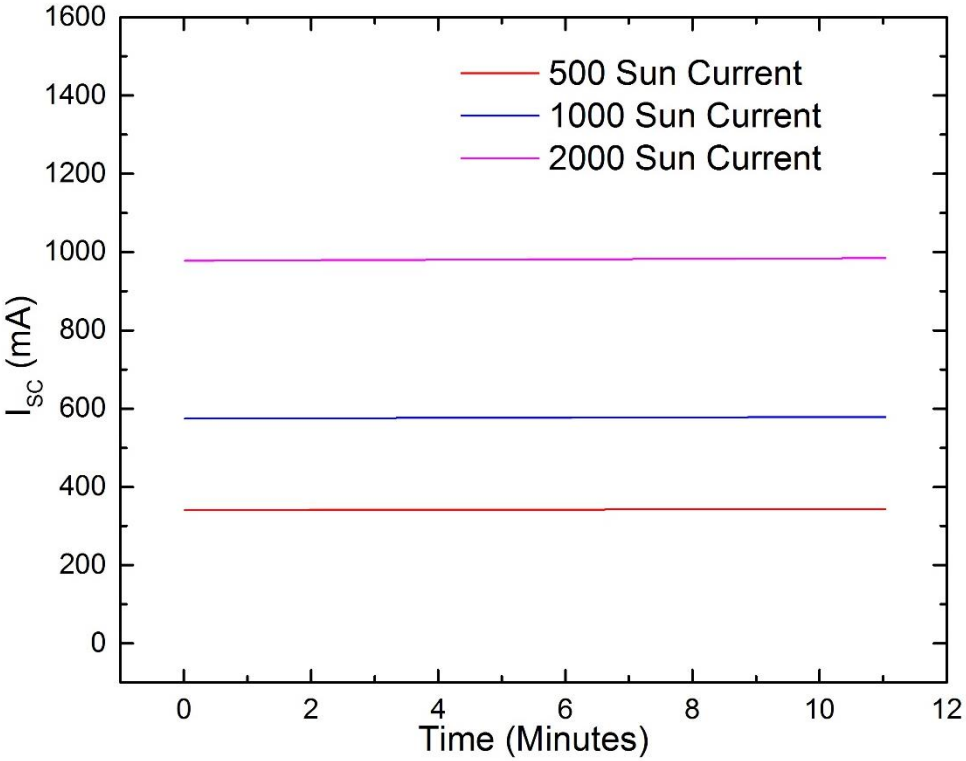

Figure 3.19: Short-Circuit current of a multi-junction solar cell under 500, 1000, and 2000 sun concentration. Reprinted with permission from Saadah, Mohammed, Edward Hernandez, and Alexander A. Balandin. "Thermal Management of Concentrated Multi-Junction Solar Cells with Graphene-Enhanced Thermal Interface Materials." Applied Sciences 7, no. 6 (2017): 589.

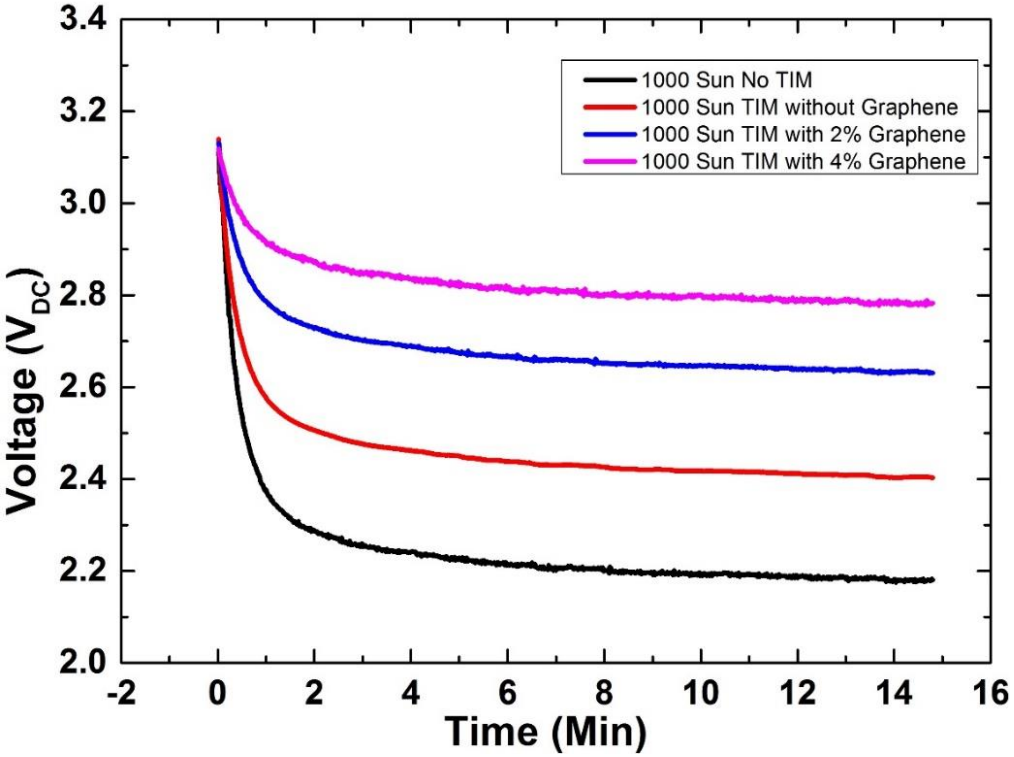

Figure 3.20: Open circuit voltage (V_{OC}) change under 1000 sun concentration without TIM and with TIM 0-4% graphene added. Reprinted with permission from Saadah, Mohammed, Edward Hernandez, and Alexander A. Balandin. "Thermal Management of Concentrated Multi-Junction Solar Cells with Graphene-Enhanced Thermal Interface Materials." Applied Sciences 7, no. 6 (2017): 589.

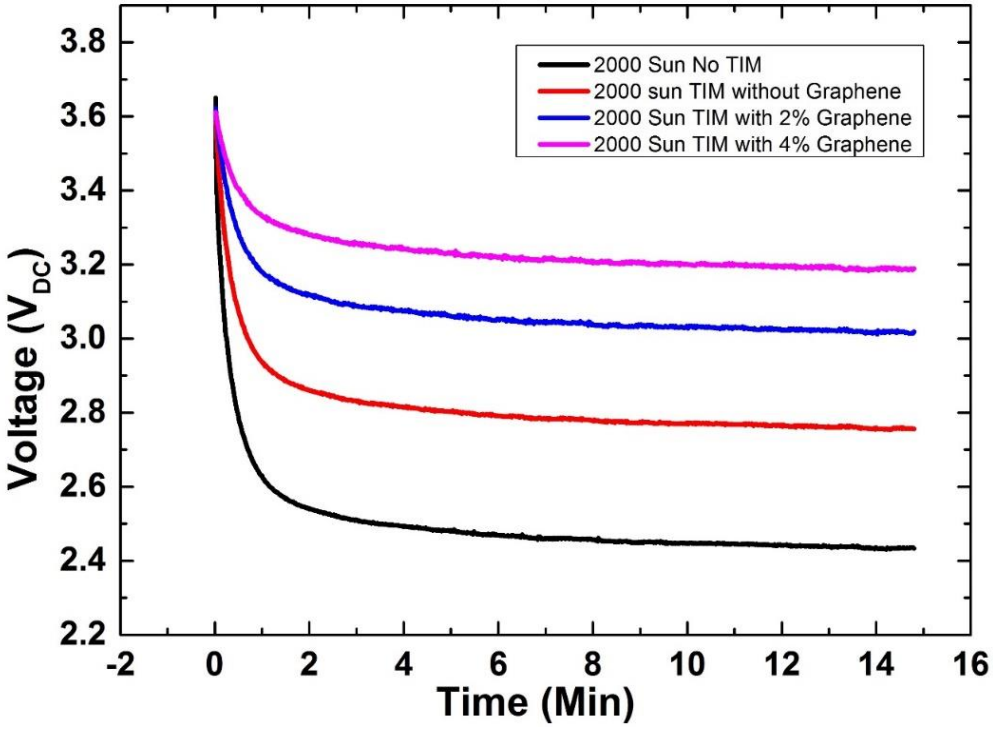

Figure 3.21: : Open circuit voltage (V_{OC}) change under 2000 sun concentration without TIM and with TIM 0-4% graphene added. Reprinted with permission from Saadah, Mohammed, Edward Hernandez, and Alexander A. Balandin. "Thermal Management of Concentrated Multi-Junction Solar Cells with Graphene-Enhanced Thermal Interface Materials." Applied Sciences 7, no. 6 (2017): 589.

3.3 TIM Tester

As mentioned in Chapter 2, the TIM Tester is a device that measures the thermal conductivities of thermal interface materials and phase change materials as well. Icefusion was mixed with 1-6 wt% of commercial 8nm flake multilayer graphene and tested with TIM tester. Results are shown in Figure 3.22. The results indicate a promising increase in thermal conductivity of up to 110% using the 6% graphene.

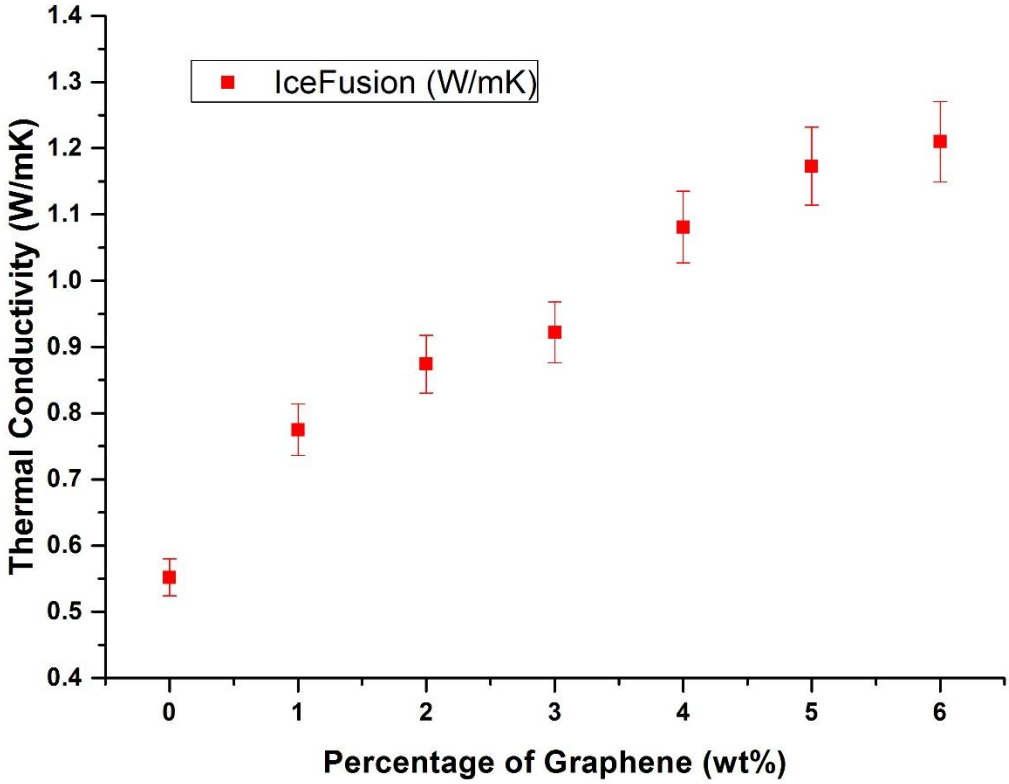

Figure 3.22: Thermal conductivity results of IceFusion with 0-6 wt% graphene as measured with the TIM Tester. Reprinted with permission from Saadah, Mohammed, Edward Hernandez, and Alexander A. Balandin. "Thermal Management of Concentrated Multi-Junction Solar Cells with Graphene-Enhanced Thermal Interface Materials." Applied Sciences 7, no. 6 (2017): 589.

Next, Arctic Alumina was also mixed with 8nm multilayer graphene using weight percentages of 1-6. The results are shown in Figure 3.23. The most improvement was obtained at around 4%, after that the thermal conductivity starts to saturate and the TIM spreads poorly when pressure applied.

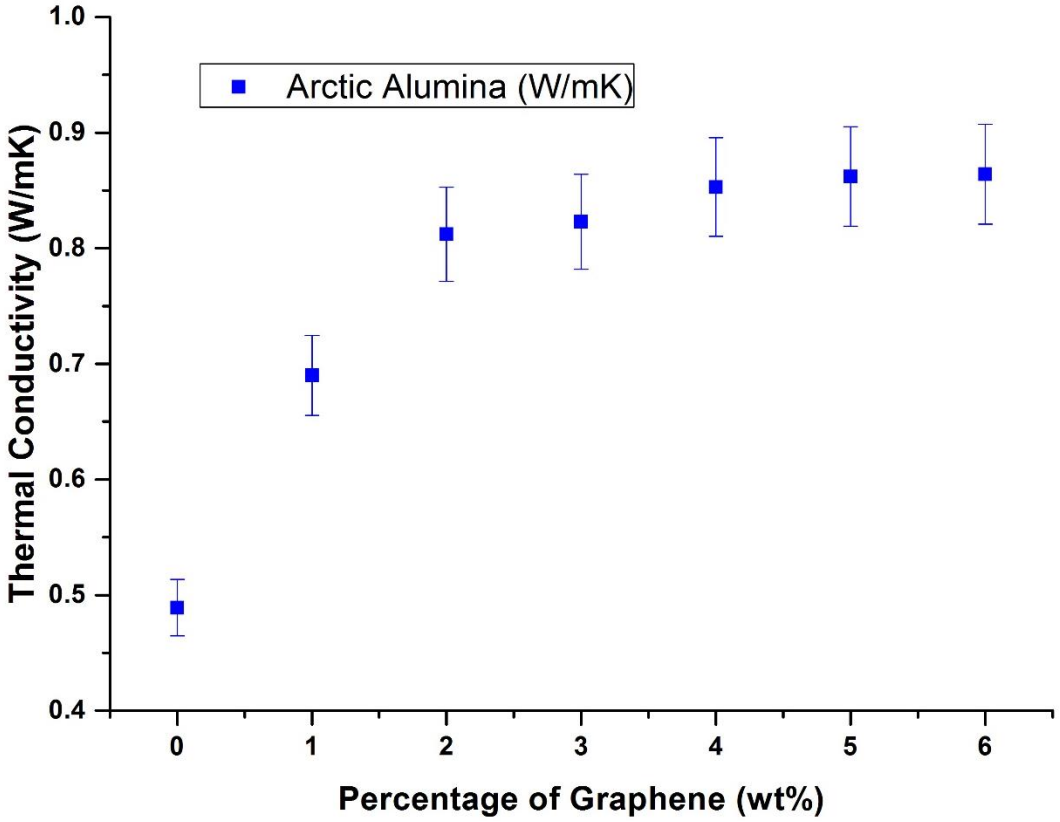

Figure 3.23: Thermal conductivity results of Arctic Alumina with 0-6 wt% graphene as measured with the TIM Tester. Reprinted with permission from Saadah, Mohammed, Edward Hernandez, and Alexander A. Balandin. "Thermal Management of Concentrated Multi-Junction Solar Cells with Graphene-Enhanced Thermal Interface Materials." Applied Sciences 7, no. 6 (2017): 589.

In contrast to the previous two TIMs, when Arctic Silver 5 was mixed with graphene it exhibits slight improvement in the first two percentages, then it saturated and

started to decline, as seen in Figure 3.24. The main reason is that the TIM became too thick to spread well and fill all the microscopic imperfections in the two adjoined surfaces.

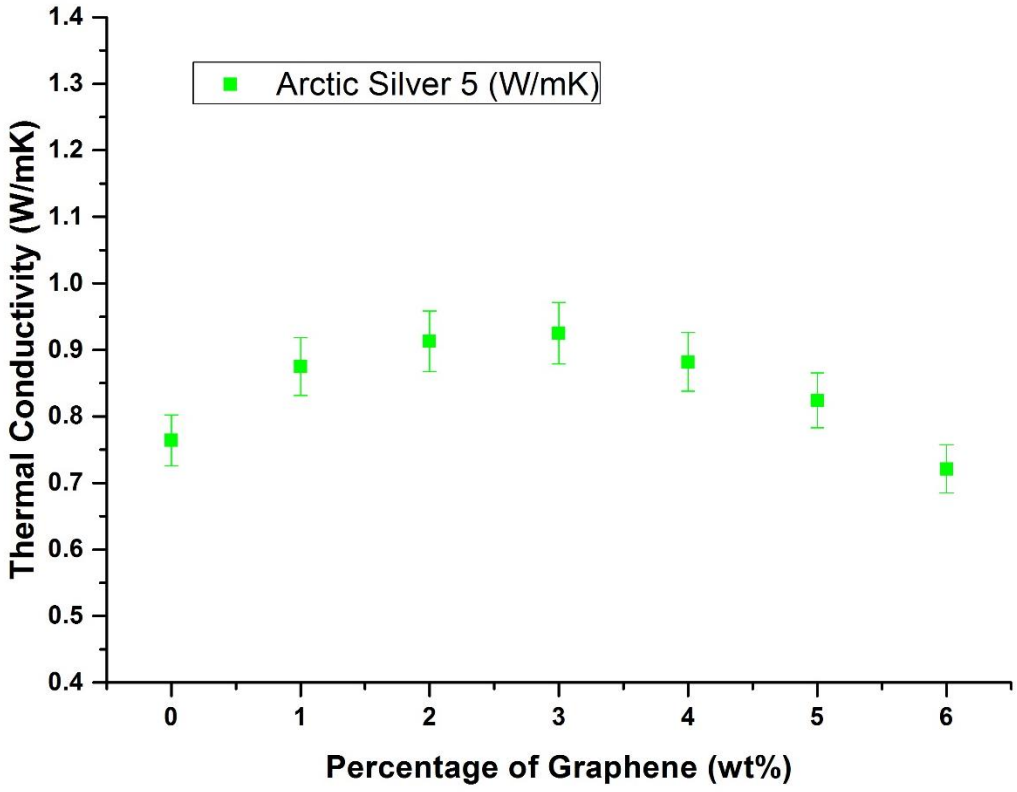

Figure 3.24: Thermal conductivity results of Arctic Silver 5 with 0-6 wt% graphene as measured with the TIM Tester. Reprinted with permission from Saadah, Mohammed, Edward Hernandez, and Alexander A. Balandin. "Thermal Management of Concentrated Multi-Junction Solar Cells with Graphene-Enhanced Thermal Interface Materials." Applied Sciences 7, no. 6 (2017): 589.

3.4 Laser Flash

As described in Chapter 2, the Laser Flash is a device that can measures the thermal conductivities, diffusivity and specific heat of thermal interface materials and phase change materials as well. Icefusion was mixed with 1-6 wt% of commercial 8nm flake multilayer graphene and tested with the laser flash instrument. Results are shown in Figure 3.25. The results shows that the laser flash reads a higher thermal conductivity than the TIM Tester and there was an increase about 90% when mixed with 6 wt% of graphene.

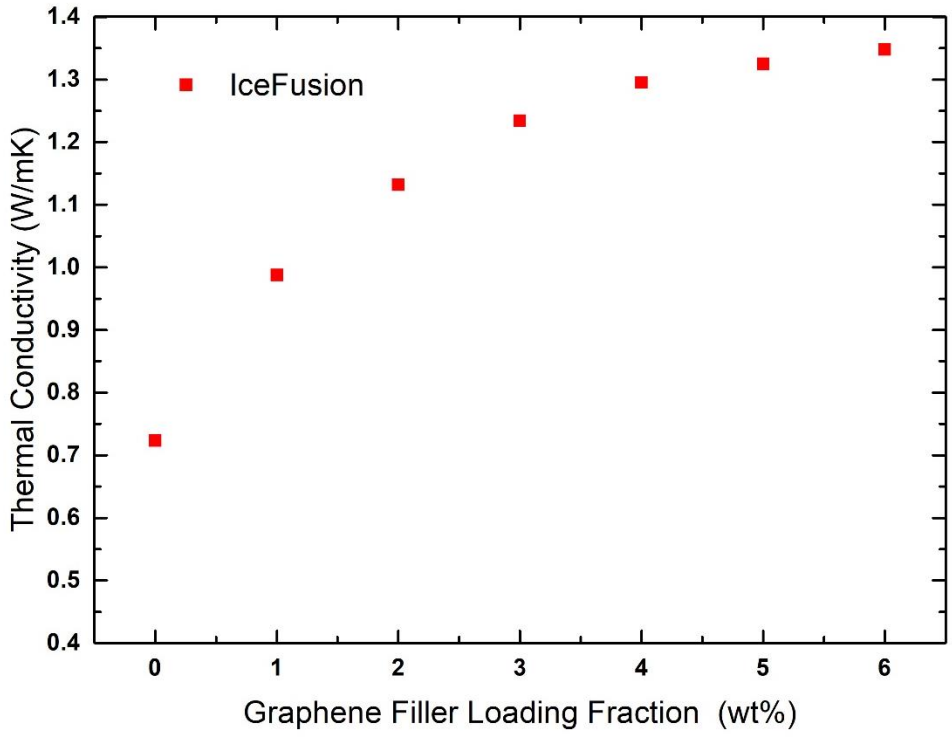

Figure 3.25: Thermal conductivity of IceFusion mixed with 1-6 wt% of graphene as tested by the laser flash instrument.

Next, Arctic Alumina was also mixed with 8nm multilayer graphene using weight fraction percentages of 1-6. The results are shown in Figure 3.26. The most improvement was obtained at around 4%, after that the thermal conductivity starts to saturate and the TIM starts to agglomerate due to high density and viscosity.

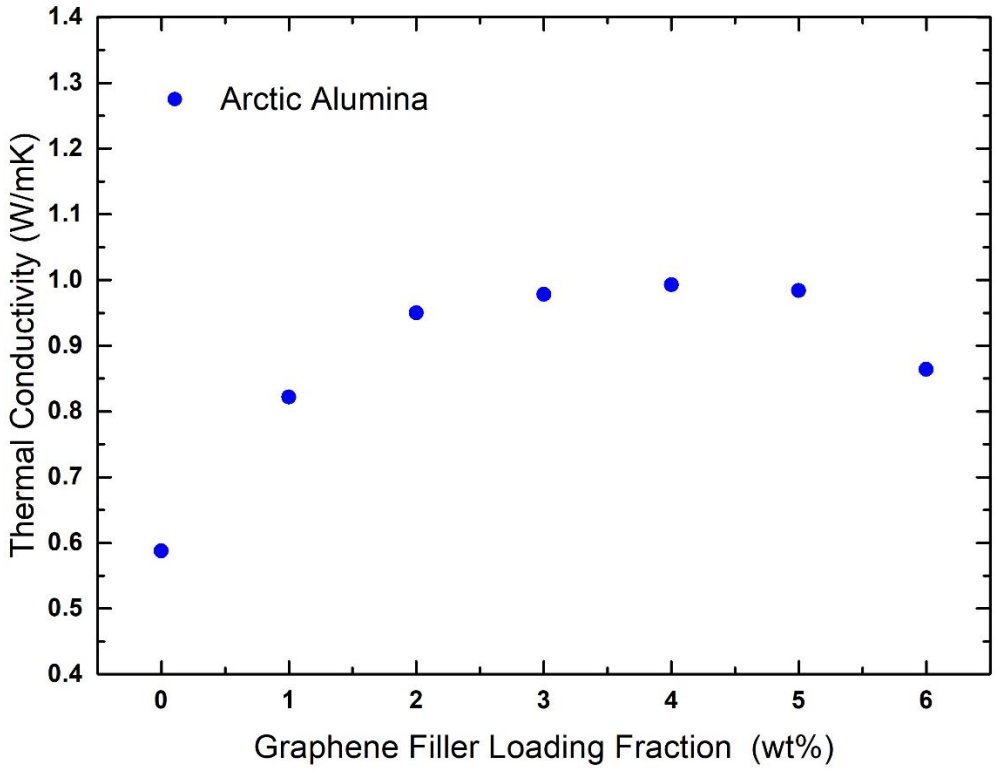

Figure 3.26: Thermal conductivity of Arctic Alumina mixed with 1-6 wt% of graphene as tested by the laser flash instrument.

Finally we have tested Arctic Silver 5 was after mixing it with graphene it exhibits slight improvement in the first two percentages, then it saturated and started to decline, as

seen in Figure 3.27, it ends up with worse thermal conductivity when mixed with 6 wt% graphene than no graphene at all. The main reason is that the TIM became too thick and dense and has high agglomeration that can cause lots of air bubbles.

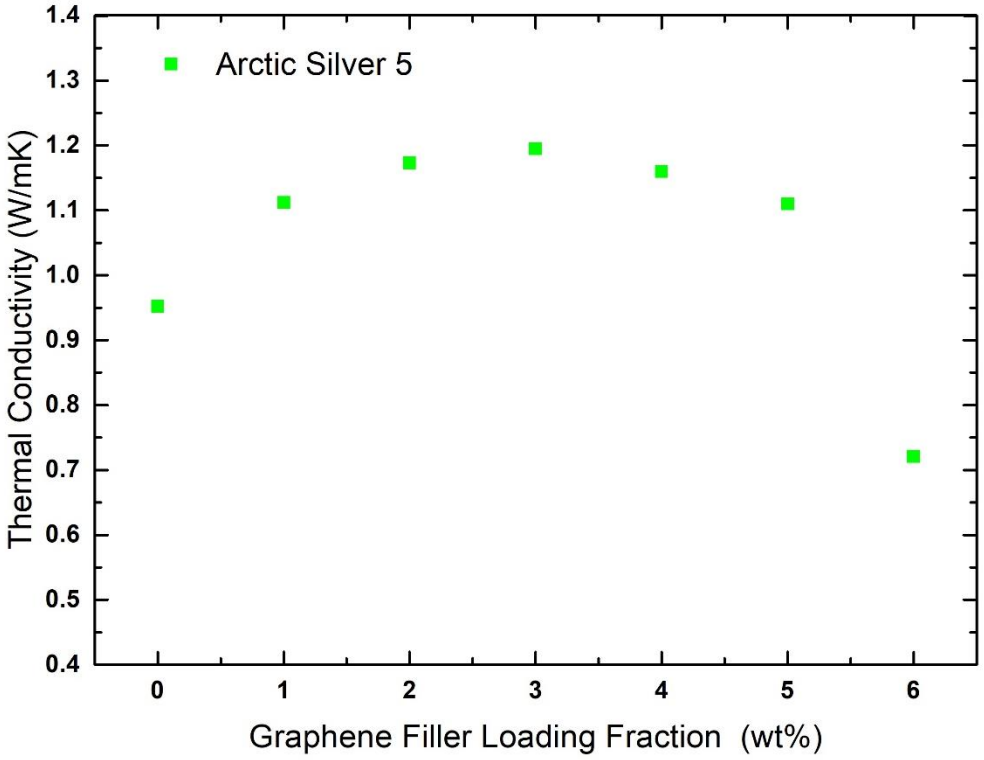

Figure 3.27: Thermal conductivity of Arctic Sliver 5 mixed with 1-6 wt% of graphene as tested by the laser flash instrument.

3.2 Discussion

Thermal interface materials aim at reducing the thermal resistance between two adjoining surfaces R_{TIM}. This resistance is affected by several factors like the TIM thermal

conductivity K_{TIM}, thermal contact resistances between the TIM and the two surfaces R_c, and the distance between the two surfaces or bond-line thickness BLT. These factors are related to R_{TIM} by the following equation:

$$R_{TIM} = \frac{BLT}{K_{TIM}} + R_{C1} + R_{C2}$$

The thermal conductivity of the TIM is affected by the filler volume fraction, the thermal conductivity of the matrix and filler, and the contact resistance between the fillers and matrix. The contact resistance between the matrix and filler can increase due to improper mixing of the filler and polymer matrix. Table 3.4 lists the physical characteristics of the three TIMs used in our study. The filler particles already existing in the base TIM, density, ΔT increase at 3 wt% of graphene, and coverage. The coverage of the base TIM is a measurement of the area in cm^2 that one gram can cover at layer thickness of 0.075 mm.

Table 3.4: Physical characteristics of the three TIMs and incrase percentage of ΔT when loaded with 3 wt% of graphene.

TIM	ρ (g/cm^3)	Filler	Coverage	ΔT
MX-4	2.5	Carbon	63	5.1%
Alumina	1.6	Al_2O_3, BN,	88	12%
Silver 5	4.1	Ag, ZnO, Al_2O_3, BN	30	2.44%
IceFusion	1.2	Al_2O_3	N/A	N/A

Arctic Silver 5 base TIM consists of 88% filler weight fraction. TIMs with high filler loading fractions generally causes an increase of BLT and K_{TIM}. With the addition of MLG the filler weight fraction was increased further and the mixed compound had a weaker spreading characteristics. It is reasonable to assume that this was the limiting factor that caused the low change in ΔT. On the other hand, the less dense and more viscous Arctic Alumina had relatively better spreading characteristics when mixed with MLG powder. With these physical differences, we were able to obtain a better and more consistent improvement of ΔT when mixing MLG with Arctic Alumina as opposed to the declining ΔT improvement with Arctic Silver 5. Figure 3.28 compares ΔT improvement as a function of graphene wt% for the three TIMs.

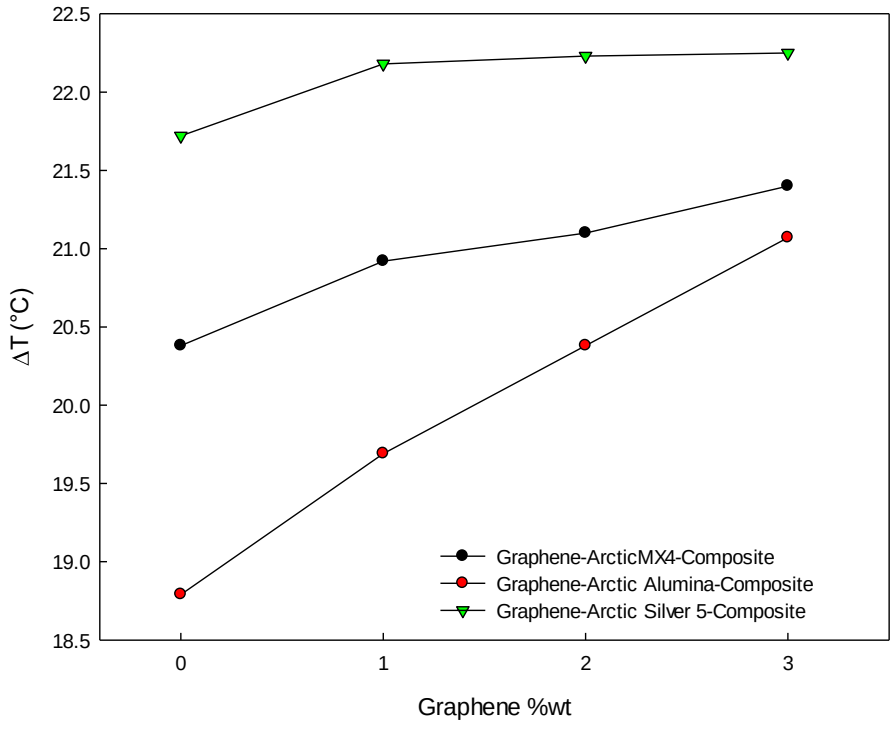

Figure 3.28: ΔT as a function of graphene weight fraction for the three tested TIMs.

The next part of our results presented the thermal interface performance in an actual solar cells under a professional solar simulator. The compound used were all made using IceFusion and graphene since they had the best improvement results under the other thermal conductivity measuring instruments. Two types of experiments conducted, a non-concentrated solar light and a concentrated solar light. It was found that a single junction power output would drop about 12% under non concentrated solar light and as much as 21% when using only 3 sun concentration. The multi junction solar cell have demonstrated that they can withstand higher concentration and perform better under high cell heat. Results have shown that using 10 suns concentration on a multi-junction will drop its output power much less than using a 3 sun concentration on a single junction solar cell. However, the multi-junction solar cells have dropped about 33% when using a very high concentration of up to 2000 suns. Both types of cells have performed much better when cooling methods employed. We were able to save as much as 65% of the power loss due to the heat by using only a 4% weight fraction of graphene with a cheap commercially available thermal interface material. It is worth noting that the 65% saved in the case of a high concentration is much more than the power saved under 1 sun concentration since the multi-junction power output would be 3.6 watt under 2000 suns compared to only 9 mW when using only one sun. That's as much as 375 times the power output, and saving 65% of the power loss would save a lot of energy especially on the long run.

The advantages of using graphene as an efficient filler for thermal interface material is augmented by testing those compound with thermal conductivity measuring instruments.

The two instruments used, TIM Tester and Laser Flash, have proven that adding a small percentage of graphene will greatly enhance the thermal conductivity of the TIM. In the case of IceFusion we were able to get 13% improvement in thermal conductivity with using only 4% graphene.

3.3 Conclusions

The dissertation described an experimental investigation of the feasibility of using graphene fillers in thermal interface materials with the goal of improving thermal management of multi-junction concentrator solar cells. Graphene and few-layer graphene fillers, produced by a scalable environmentally-friendly liquid-phase exfoliation technique, were incorporated into conventional thermal interface materials. Characteristics of the composites have been examined with Raman spectroscopy, optical microscopy and thermal conductivity measurements. Graphene-enhanced thermal interface materials have been applied between a solar cell and heat sink to improve heat dissipation. The performance of the single and multi-junction solar cells has been tested using an industry-standard solar simulator under the light concentration of up to 2000 suns. It was found that the application of graphene-enhanced thermal interface materials allows one to reduce the solar cell temperature and increase the open-circuit voltage. The results of the dissertation demonstrated that the use of graphene helps in recovering significant amount of the power loss due to solar cell overheating. The obtained results are important for the development

of new technologies for thermal management of concentrated and multi-junction photovoltaic solar cells."

The dissertation also presented the results of experimental approaches to improve thermal interface conductance between solar cells and heat spreaders by developing better thermal interface materials. Three major commercial TIMs were mixed with multi-layer graphene nano-powder at different weight fractions and tested a solar cell module. The performance of the three TIMs were improved with the graphene addition. Physical properties of the base TIMs, like density, viscosity, and filler loading fractions were factors in determining the level of performance increase of the hybrid MLG-TIM compounds. TIMs that have lower density, less volume loading fraction, and higher viscosity gave better and steadier thermal performance when mixed with graphene.

References

[1] Masuko, Keiichiro, Masato Shigematsu, Taiki Hashiguchi, Daisuke Fujishima, Motohide Kai, Naoki Yoshimura, Tsutomu Yamaguchi et al. "Achievement of more than 25% conversion efficiency with crystalline silicon heterojunction solar cell." *IEEE Journal of Photovoltaics* 4, no. 6 (2014): 1433-1435.

[2] Sohrabi, Foozieh, Arash Nikniazi, and Hossein Movla. 2013. “Optimization of Third Generation Nanostructured Silicon-Based Solar Cells.” *Solar Cells - Research and Application Perspectives - InTech* 1: 1–26. do:10.5772/51616. doi:10.5772/51616.

[3] Yong S.Cho, Howard D Glicksman and Vasantha R W Amarakoon. 2004. “Encyclopedia of Nanoscience and Nanotechnology.” *Ceramic Nanopowders* 1 (1): 727. doi:10.1081/E-ENN.

[4] Sark, Wilfried Van, Lars Korte, and Francesco Roca. 2012. “Introduction – Physics and Technology of Amorphous-Crystalline Heterostructure Silicon.” *Physics and Technology of Amorphous-Crystalline Heterostructure Silicon Solar Cells*, 1–12. doi:10.1007/978-3-642-22275-7.

[5] Snaith, Henry J. "Perovskites: the emergence of a new era for low-cost, high-efficiency solar cells." *The Journal of Physical Chemistry Letters* 4, no. 21 (2013): 3623-3630.

[6] Lee, Michael M., Joël Teuscher, Tsutomu Miyasaka, Takurou N. Murakami, and Henry J. Snaith. "Efficient hybrid solar cells based on meso-superstructured organometal halide perovskites." *Science* 338, no. 6107 (2012): 643-647.

[7] Kojima, Akihiro, Kenjiro Teshima, Yasuo Shirai, and Tsutomu Miyasaka. "Organometal halide perovskites as visible-light sensitizers for photovoltaic cells." *Journal of the American Chemical Society* 131, no. 17 (2009): 6050-6051.

[8] Becker, Christiane, Daniel Amkreutz, Tobias Sontheimer, Veit Preidel, Daniel Lockau, Jan Haschke, Lisa Jogschies et al. "Polycrystalline silicon thin-film solar cells: Status and perspectives." *Solar Energy Materials and Solar Cells*119 (2013): 112-123.

[9] Konagai, Makoto. "Present status and future prospects of silicon thin-film solar cells." *Japanese Journal of Applied Physics* 50, no. 3R (2011): 030001.

[10] Avrutin, V., N. Izyumskaya, and H. Morkoç. "Semiconductor solar cells: Recent progress in terrestrial applications." *Superlattices and Microstructures*49, no. 4 (2011): 337-364.

[11] Tyagi, V. V., Nurul AA Rahim, N. A. Rahim, A. Jeyraj, and L. Selvaraj. "Progress in solar PV technology: Research and achievement." *Renewable and sustainable energy reviews* 20 (2013): 443-461.

[12] Saadah, M., D. Gamalath, E. Hernandez, and A. A. Balandin. "Graphene-enhanced thermal interface materials for heat removal from photovoltaic solar cells." In *SPIE Nanoscience+ Engineering*, pp. 99320H-99320H. International Society for Optics and Photonics, 2016.

[13] Guter, Wolfgang, Jan Schöne, Simon P. Philipps, Marc Steiner, Gerald Siefer, Alexander Wekkeli, Elke Welser, Eduard Oliva, Andreas W. Bett, and Frank Dimroth. "Current-matched triple-junction solar cell reaching 41.1% conversion efficiency under concentrated sunlight." *Applied Physics Letters*94, no. 22 (2009): 223504.

[14] Dimroth, Frank, Matthias Grave, Paul Beutel, Ulrich Fiedeler, Christian Karcher, Thomas ND Tibbits, Eduard Oliva et al. "Wafer bonded four-junction GaInP/GaAs//GaInAsP/GaInAs concentrator solar cells with 44.7% efficiency." *Progress in Photovoltaics: Research and Applications* 22, no. 3 (2014): 277-282.

[15] Dahal, R., J. Li, K. Aryal, J. Y. Lin, and H. X. Jiang. "InGaN/GaN multiple quantum well concentrator solar cells." *Applied Physics Letters* 97, no. 7 (2010): 073115.

[16] Wheeldon, Jeffrey F., Christopher E. Valdivia, Alexandre W. Walker, Gitanjali Kolhatkar, Abdelatif Jaouad, Artur Turala, Bruno Riel et al. "Performance comparison of AlGaAs, GaAs and InGaP tunnel junctions for concentrated multijunction solar cells." *Progress in Photovoltaics: Research and Applications* 19, no. 4 (2011): 442-452.

[17] Lee, Seri. "Thermal challenges and opportunities in concentrated photovoltaics." In *Electronics Packaging Technology Conference (EPTC), 2010 12th*, pp. 608-613. IEEE, 2010.

[18] Buljan, Marina, João Mendes-Lopes, Pablo Benítez, and Juan Carlos Miñano. "Recent trends in concentrated photovoltaics concentrators' architecture." *Journal of Photonics for Energy* 4, no. 1 (2014): 040995-040995.

[19] Tromholt, Thomas, Eugene A. Katz, Baruch Hirsch, Alexis Vossier, and Frederik C. Krebs. "Effects of concentrated sunlight on organic photovoltaics." *Applied Physics Letters* 96, no. 7 (2010): 073501.

[20] Barlev, David, Ruxandra Vidu, and Pieter Stroeve. "Innovation in concentrated solar power." *Solar Energy Materials and Solar Cells* 95, no. 10 (2011): 2703-2725.

[21] Chemisana, Daniel. "Building integrated concentrating photovoltaics: a review." *Renewable and Sustainable Energy Reviews* 15, no. 1 (2011): 603-611.

[22] Saadah, Mohammed, Edward Hernandez, and Alexander A. Balandin. "Thermal Management of Concentrated Multi-Junction Solar Cells with Graphene-Enhanced Thermal Interface Materials." *Applied Sciences* 7, no. 6 (2017): 589.